Calibration of a large-scale hydrological model using satellite-based soil moisture and evapotranspiration products

Patricia López López[1,2], Edwin H. Sutanudjaja[2], Jaap Schellekens[1], Geert Sterk[2], and Marc F. P. Bierkens[2,3]

[1]Deltares, Delft, the Netherlands
[2]Department of Physical Geography, Faculty of Geosciences, Utrecht University, Utrecht, the Netherlands
[3]Deltares, Utrecht, the Netherlands

Correspondence to: Patricia López López (patricia.lopez@deltares.nl)

Abstract.

A considerable number of river basins around the world lack sufficient ground observations of hydro-meteorological data for effective water resources assessment and management. Several approaches can be developed to increase the quality and availability of data in these poorly gauged or ungauged river basins, and among those, the use of earth observations products has recently become promising. Earth observations of various environmental variables can be used potentially to increase the knowledge about the hydrological processes in the basin and to improve streamflow model estimates, via assimilation or calibration. The present study aims to calibrate the large-scale hydrological model PCR-GLOBWB using satellite-based products of evapotranspiration and soil moisture for the Moroccan Oum Er Rbia basin. Daily simulations at a spatial resolution of 5 arcmin x 5 arcmin are performed with varying parameters values for the 32-year period 1979-2010. Five different calibration scenarios are inter-compared: (i) reference scenario using the hydrological model with the standard parameterization, ii) calibration using in-situ observed discharge time series, (iii) calibration using GLEAM actual evapotranspiration time series, (iv) calibration using ESA CCI surface soil moisture time series and (v) step-wise calibration using GLEAM actual evapotranspiration and ESA CCI surface soil moisture time series. The impact on discharge estimates of precipitation in comparison with model parameters calibration is investigated using three global precipitation products, including EI, WFDEI and MSWEP.

Results show that GLEAM evapotranspiration and ESA CCI soil moisture may be used for model calibration resulting in reasonable discharge estimates (NSE values from 0.5 to 0.75), although better model performance is achieved when the model is calibrated with in-situ streamflow observations. Independent calibration based on only evapotranspiration or soil moisture observations improves model predictions to a lesser extent. Precipitation input affects to discharge estimates more than calibrating model parameters. The use of WFDEI precipitation leads to the lowest model performances. Apart from the in-situ discharge calibration scenario, the highest discharge improvement is obtained when EI and MSWEP precipitation products are used in combination with a step-wise calibration approach based on evapotranspiration and soil moisture observations. This study opens up the possibility to use globally available earth observations and reanalysis products of precipitation, evapotranspiration and soil moisture into large-scale hydrological models to estimate discharge at a river basin scale.

1 Introduction

To assess and manage the available water resources within a river basin, good estimates of hydro-meteorological data, such as precipitation, temperature and streamflow, are required. Yet many river basins around the world still have a limited number of in-situ observations, being either ungauged (Sivapalan et al., 2003) or poorly gauged (Loukas and Vasiliades, 2014). Ungauged or poorly gauged river basins also include those basins where data are inaccurate, scarce, intermittent or collected at different temporal resolutions, leading to the problem that it is not clear how to integrate these data consistently into hydrological models (Winsemius et al., 2009). As a result, the limited availability and poor quality of data induces large uncertainty in model outputs from these river basins (Seibert and Beven, 2009). Developing novel strategies to enhance available datasets and hydrological models is one of the key strategies when working in ungauged basins (Hrachowitz et al., 2013).

To overcome the lack of hydro-meteorological data, a promising approach is the use of the recently developed global earth observations and reanalysis products to supplement the available data. In the last decades, radar and satellite technologies have improved and have become more broadly available providing diverse hydro-meteorological datasets at finer spatial and temporal resolutions: precipitation -CMORPH (Joyce et al., 2004); TRMM (Huffman et al., 2007); etc.-, soil moisture -AMSR-E (Njoku et al., 2003); ESA-CCI (Dorigo et al., 2015); etc.-, total water storage -GRACE (Tapley et al., 2004); etc.-, evapotranspiration -SEBAL (Bastiaanssen et al., 1998); MOD16 (Nishida, 2003); GLEAM (Miralles et al., 2011b); etc.-, etc.

Previous studies have demonstrated the possibility of using these global datasets to better understand the hydrological processes in a river catchment (Kite and Droogers, 2000; Vereecken et al., 2008; Seneviratne et al., 2010; Hafeez et al., 2011) and to improve streamflow model estimates through assimilation (e.g. surface soil moisture - Parajka et al., 2006; Brocca et al., 2012; López López et al., 2016 - or snow cover - Roy et al., 2010; Thirel et al., 2013 -) and/or calibration techniques or a-priori determination of model parameters (e.g. Jacobs et al., 2003; Beck et al., 2009). Calibration approaches based on multiple remotely sensed variables have some advantages in comparison with traditional calibration approaches using only observed and modelled hydrographs in a limited number of locations. Fenicia et al. (2007) and Gupta et al. (2008) recognized that traditional calibration may lead to over-parameterization, i. e. similar model results are obtained with more than one parameters combination, whereas calibrating to multiple variables - step-wise calibration - may partly resolve the problem of non-uniqueness and it helps to a better understanding of the processes happening within the catchment.

Several studies have investigated calibration approaches based on variables different to streamflow. Campo et al. (2006) used soil moisture information from radar images from ERS-2 sensors to parameterize the hydrological model MOBIDIC. Immerzeel and Droogers (2008) calibrated the hydrological model SWAT based on satellite evapotranspiration from MODIS satellite images. Lo et al. (2010) improved the parameter estimation of the Community Land Model 3.0. using GRACE total water storage data while Isenstein et al. (2015) calibrated the VIC hydrological model using snow covered area from MODIS satellite data. Others have combined remotely sensed variables with in-situ streamflow observations for calibration. In Rientjes et al. (2013), the HBV model was calibrated on satellite based evapotranspiration from MODIS and streamflow. Wanders et al. (2014) calibrated model parameters of LISFLOOD based on discharge and soil moisture observations acquired by AMSR-E, SMOS and ASCAT while Sutanudjaja et al. (2014) calibrated the large-scale model PCR-GLOBWB using streamflow and

soil water index information derived from the ERS scatterometers. At a global scale, Beck et al. (2016a) used parameter regionalization to calibrate a HBV model. However, the simultaneous use of more than one environmental variable different to streamflow for calibration is rare. A calibration approach using various variables, independently and in combination with streamflow observations, may further improve model performance and contribute to a better understanding of hydrological processes. In the present study, this is tested by comparing multiple calibration scenarios based on evapotranspiration, soil moisture and discharge data.

The previously mentioned calibration experiments were performed for well studied river basins, such as the Rhine-Meuse river basin, with a good coverage of in-situ hydro-meteorological data. In the present study area, the Oum Er Rbia river basin located in Morocco, ground observations are spatially sparse and limited in number classifying it as a poorly-gauged river basin. The region frequently suffers from water scarcity and droughts and water availability is the main factor influencing socio-economic development, mostly driven by the agriculture (Houdret, 2008). The studies of Tramblay et al. (2012), Tramblay et al. (2016) and Ouatiki et al. (2017) are testimony to the relevance of this area. Therefore, developing new strategies to model this watershed is highly relevant to improve water management and assessment of the water availability within the basin.

This study aims to calibrate a large-scale hydrological model (PCR-GLOBWB 2.0, https://github.com/UU-Hydro/PCR-GLOBWB_model, Sutanudjaja et al., 2016) using soil moisture and evapotranspiration observations alone and to compare its discharge estimates to those obtained when the model is traditionally calibrated to streamflow data. We use the evapotranspiration product generated by an enhanced version of the GLEAM model (GLEAM v3.0; Martens et al., 2016b) in combination with the surface soil moisture product from ESA CCI (Dorigo et al., 2015). Both products are derived from satellite data. Furthermore, the influence of precipitation forcing is considered and three different global precipitation products are used and inter-compared: ERA-Interim reanalysis data (EI, Dee et al., 2011), WATCH Forcing Data methodology applied to ERA-Interim reanalysis data, (WFDEI, Weedon et al., 2014) and Multi-Source Weighted-Ensemble Precipitation data by merging gauge, satellite and reanalysis data (MSWEP, Beck et al., 2016b).

Five different calibration approaches are performed by using five calibration scenarios that include streamflow, soil moisture and evapotranspiration: (i) reference scenario using the hydrological model with the standard parameterization, (ii) calibration using in-situ observed discharge time series, (iii) calibration using GLEAM actual evapotranspiration time series, (iv) calibration using ESA CCI surface soil moisture time series and (v) step-wise calibration using GLEAM actual evapotranspiration and ESA CCI surface soil moisture time series. The above is repeated for each of the selected global precipitation product. A priori, it is expected that calibrating to streamflow observations yields the best discharge estimates, and that the step-wise calibration using soil moisture and evapotranspiration provides better results than the calibration scenarios based only on soil moisture or evapotranspiration.

The novel aspects and new contributions of this work include the use and comparison of three different and recently generated global precipitation products, the exploration of calibration techniques based on earth observations of soil moisture and evapotranspiration and their application into a large-scale hydrological model to provide streamflow estimates in the ungauged river basin of Oum Er Rbia in Morocco. Furthermore, understanding the potential gain of calibrating large-scale models to remotely sensed observations may have benefits for water resources management in data-poor river basins globally.

This manuscript first describes the study area, then the methodology, including the hydrological model, the data, the calibration and validation strategy and the performance metrics. Subsequently, results are presented, starting with the inter-comparison of precipitation products and following with calibration and validation results. This manuscript ends with discussion and conclusions.

2 Study area

The study area is the Oum Er Rbia River basin, which is situated in the central-west region of Morocco between the Atlas Mountains to the south and the Mesetian area to the north flowing into the Atlantic Ocean (Figure 1). The basin's topography ranges from 2,800 m in the southern upstream zone to 150 m in the northern downstream zone. The Oum Er Rbia is the second largest river in Morocco with a total length of 550 km and it drains an area of approximately 38,025 km^2.

The climate in the coastal and mountainous areas is Mediterranean, characterized with high temperatures in the summer and warm autumn and winter months with rainfall, and semi-arid in the central plain (Jones et al., 2013). Precipitation increases from downstream to upstream areas in the mountains. The mean annual precipitation and temperature are 400 mm and 18$^{\mathrm{o}}\mathrm{C}$, respectively. Approximately 70 % to 80 % of the annual rainfall is concentrated in the period from October to May.

The lowlands of the basin are mainly covered with rain-fed and irrigated agriculture fields and the upstream regions are a combination of Mediterranean forests, woodlands and scrubs. The geology of the area is mostly composed of limestone, marls and sandstone with a karst aquifer in the Atlas Mountains and a multi-layered system of superficial and deep aquifers in the western plains (Bouchaou et al., 2009).

3 Methodology

3.1 Large-scale hydrological model: PCR-GLOBWB

The large-scale hydrological model PCR-GLOBWB 2.0 (https://github.com/UU-Hydro/PCR-GLOBWB_model, Sutanudjaja et al., 2016) was used at a spatial resolution of 5 arcmin x 5 arcmin (approximately 10 km x 10 km at the equator) and at a daily temporal resolution. PCR-GLOBWB is a leaky-bucket type of model applied on a cell-by-cell basis. Figure 2 illustrates a schematic representation of the structure of PCR-GLOBWB model. For each grid cell and time step, the model determines the water balance considering the following water storage components: soil moisture, groundwater, surface water, interception storage and snow. The soil is divided into three vertical layers representing the top 5 cm of soil (depth $Z_1 \leq 5$ cm), the following 25 cm of soil (depth $Z_2 \leq 30$ cm) and the remaining 120 cm of soil (depth $Z_3 \leq 150$ cm), in which the storages are symbolized as S_1, S_2 and S_3, respectively. The underlying groundwater store (S_4) consists of two layers: an active or renewable layer and a non-active or non-renewable layer of fossil water, in which the storages are symbolized as $S_{4\mathrm{act}}$ and $S_{4\mathrm{fos}}$, respectively. The model also includes the water exchange processes between the top layer and the atmosphere (precipitation, evapotranspiration and snowmelt), between the soil layers (percolation and capillary rise) and between the soil layers and the active layer of the groundwater store (groundwater recharge, discharge to baseflow and capillary rise). Each grid cell is divided into sub-grids

considering variations of elevation, vegetation, soil and land cover. Five land cover types are distinguished: irrigated paddy field, irrigated non-paddy field, grassland (short natural vegetation), forest (tall natural vegetation) and open water. To compute the total runoff of every grid cell, the model includes direct runoff (Q_{DR}), shallow sub-surface flow from the third soil layer (Q_{SF}), and baseflow from the active groundwater layer (Q_{BF}). The total runoff is accumulated from all grid cells and routed along the drainage network to obtain the river discharge (Q_{channel}). The PCR-GLOBWB model version used here (Sutanudjaja et al., 2016) simulates water availability and water abstraction, including reservoirs and domestic, industrial, livestock and irrigational water demands. The following subsections briefly describe the model components and the parameters relevant for the present calibration study. The reader is referred to Sutanudjaja et al. (2011) and Sutanudjaja et al. (2014) for a more detailed explanation.

3.1.1 Direct or surface runoff

The amount of water that goes into the soil is the net precipitation (P_n) resulting from the surplus of precipitation above the interception capacity and the excess melt water from the snow pack. P_n is partitioned into direct runoff (Q_{DR}) and net infiltration to the first soil layer (P_{01}). The partitioning is done using the Improved Arno Scheme (Hagemann and Gates, 2003), in which the fraction of saturated soil of a cell is estimated based on the cell-minimum capacity (W_{min}), the cell-average actual storage (W_{act}=S_1+S_2+S_3) and the water capacity for the entire soil profile (W_{max}= SC_1+SC_2+SC_3, SC_n: soil water capacity for layer n). If $W_{\text{min}} = 0$, direct runoff always occurs for a rainfall event. If $W_{\text{min}} > 0$, an event P_n only generates runoff Q_{DR} if $W_{\text{act}} > W_{\text{min}}$. W_{min} is therefore an important parameter which governs runoff generation response time.

3.1.2 Vertical water exchanges between soil and groundwater stores and shallow sub-surface flow

Net infiltration water into the first soil layer (P_{01}) is transferred through the remaining soil layers. Vertical water exchanges occur between the first and the second layers (P_{12}), between the second and the third layers (P_{23}) and between the third soil layer and the active layer of the groundwater store (P_{34}). P_{12},P_{23} and P_{34} consist of downward percolation and upward capillary rise, which depend on the degree of saturation ($s_1 = S_1/SC_1$,$s_2 = S_2/SC_2$ and $s_3 = S_3/SC_3$) and the unsaturated hydraulic conductivity of each soil layer ($K_{\text{sat 1}}$,$K_{\text{sat 2}}$ and $K_{\text{sat 3}}$). If s_1>s_2 , percolation is equal to $K_{\text{sat 1}}$; whereas if s_2>s_1, capillary rise is equal to $K_{\text{sat 2}} \times (1 - s_1)$, being $(1 - s_1)$ the moisture deficit in the first soil layer. $K_{\text{sat 1}}$, $K_{\text{sat 2}}$ and $K_{\text{sat 3}}$ controls the vertical fluxes between the soil layers and the groundwater store which affect significantly to the ground water recharge. Moreover, $K_{\text{sat 3}}$ influences the shallow sub-surface flow from the third soil layer (Q_{IF}).

3.1.3 Baseflow

The last component that contributes to the total runoff for each grid cell is the baseflow from the active groundwater layer (Q_{BF}). Q_{BF} is calculated as $Q_{\text{BF}} = S_{4\text{act}} \times J$, where J is the baseflow recession coefficient and depends on the aquifer transmissivity and the aquifer specific yield. Therefore, J controls the direct contribution of groundwater store to the total runoff and hence, to the river discharge.

3.1.4 Evapotranspiration

Actual evapotranspiration consist of transpiration (E_t), bare soil evaporation from the top soil layer (E_b), open-water evaporation (E_w), interception loss (E_i) and evaporation from the melt water store in the snow pack (E_s). Each evapotranspiration component is calculated using the reference potential evapotranspiration ($E_{(p,0)}$) as basis and the corresponding factor coefficients related with vegetation cover fraction, crop and land cover type, surface water bodies, water stress and the interception flux.

3.2 Data

3.2.1 Meteorological data

The meteorological data required to force PCR-GLOBWB are air temperature, precipitation and reference potential evapotranspiration. Air temperature and precipitation were obtained from the WATCH Forcing Data methodology applied to ERA-Interim reanalysis data (WFDEI) at an original spatial resolution of 0.5^o x 0.5^o (Weedon et al., 2014). Reference potential evapotranspiration was obtained through the FAO Penman-Monteith equation. Precipitation, air temperature and reference potential evapotranspiration were downscaled from the original spatial resolution to a 0.08^o x 0.08^o grid. Precipitation and air temperature were downscaled using precipitation and temperature lapse rates derived from the 10' CRU-CL2.0 data (New et al., 2002) through a linear regression analysis (Sutanudjaja et al., 2011). Reference potential evapotranspiration was downscaled using the e2o-downscaling-tools (Weiland et al., 2015; Schellekens and Weiland, 2017).

To test model sensitivity to precipitation, air temperature and reference potential evapotranspiration were fixed and two additional global precipitation products were used: (i) ERA-Interim reanalysis data (EI) from the European Centre for Medium-range Weather Forecasts (ECMWF) at the original spatial resolution of 0.5^o x 0.5^o (Dee et al., 2011) and (ii) Multi-Source Weighted-Ensemble Precipitation data (MSWEP) by merging gauge, satellite and reanalysis data at the original spatial resolution of 0.25^o x 0.25^o (Beck et al., 2016b).

The three global precipitation products were inter-compared and interpolated to the two weather station locations found inside the Oum Er Rbia basin (http://www.wmo.int/pages/themes/climate/), Beni Mellal and Kasba Tadla (Figure 1). Kling-Gupta efficiency (KGE), Nash-Sutcliffe efficiency (NSE), Pearson's correlation coefficient (r) and Percent Bias ($PBias$) between the interpolated and in-situ ground daily data were calculated. A description of the performance metrics with their mathematical formulation is included in section 3.4. These metrics were selected to have detailed information about differences between precipitation products.

3.2.2 Discharge data

Daily river gauge data were obtained from the Oum Er Rbia Hydraulic Agency (ABHOER). Gauge measurements from two gauges in the western region of the basin were used in this study (Figure 1): Ait Ouchene and Mechra Eddahk. Table 1 summarizes some key hydrological data.

3.2.3 Evapotranspiration data

The GLEAM (Global Land Evaporation Amsterdam Model - http://www.gleam.eu/ -) evapotranspiration product version 3.0a (GLEAM_v3.0a), generated by VU Amsterdam in collaboration with Ghent University (Miralles et al., 2011b;Miralles et al., 2011a; Martens et al., 2016b), was used to calibrate PCR-GLOBWB. The product consists of a global dataset based on reanalysis net radiation and air temperature, satellite and gauged-based precipitation, Vegetation Optical Depth (VOD) and snow water equivalents spanning the 35-year period 1980-2014. To generate the GLEAM evapotranspiration product, the GLEAM model separately estimates the different components of terrestrial evaporation, including transpiration, interception loss, bare-soil evaporation, snow sublimation and open-water evaporation. To this end, it consists of four modules: the evaporation module, the stress module, the soil-water balance module and the rainfall interception model (Martens et al., 2016a). GLEAM (0.25^o x 0.25^o) was interpolated with distance-weighted average remapping to a 0.08^o x 0.08^o grid for the period 1980-2010. GLEAM actual evapotranspiration thus obtained was subsequently compared to simulated actual evapotranspiration by PCR-GLOBWB.

3.2.4 Soil moisture data

The ESA CCI surface soil moisture combined product version 2.2 (ESA CCI SM v02.2 CP) was generated as part of the European Space Agency (ESA) soil moisture Climate Change Initiative (CCI) project by the Vienna University of Technology (http://www.esasoilmoisture-cci.org/). A dataset for the 35-year period 1980-2014 of surface soil moisture was produced using C-band scatterometer data (ERS-1/2 AMI scatterometer, MetOp Advanced Scatterometer -ASCAT-) and multi-frequency radiometer data (SMMR, SSM/I, TMI, AMSR-E, Windsat and AMSR2). Soil moisture retrieved using satellite active microwave data and satellite microwave radiometry were merged to make best use of soil moisture data from the different available satellites and sensors (Liu et al., 2011; Liu et al., 2012; Dorigo et al., 2015). ESA CCI surface soil moisture combined product represents approximately a top soil layer depth of 0.5 - 2 cm. Similarly to GLEAM evapotranspiration, ESA CCI SM product at an original spatial resolution of 0.25^o x 0.25^o was interpolated with distance-weighted average remapping to 0.08^o x 0.08^o grid for the period 1980-2010.

ESA CCI surface soil moisture observations were compared to simulated soil moisture of the first of the three vertical soil layers in PCR-GLOBWB (top 5 cm of soil). Due to differences in layer depth and/or data characteristics, systematic biases between modelled and observed soil moisture may exist (Reichle and Koster, 2004). To overcome this expected discrepancy and match the remotely sensed observations to the statistics of corresponding hydrological model simulations, a mean-standard deviation ($\mu - \sigma$) matching (Draper et al., 2009) was used. This technique was implemented to rescale simulated soil moisture against ESA CCI surface soil moisture time series to have the same mean and variance.

The adjusted simulated surface soil moisture values $\theta^{'}_{sim}$ were calculated as

$$\theta^{'}_{sim} = \frac{\sigma_{\theta_{obs}}}{\sigma_{\theta_{sim}}} \times (\theta_{sim} - \overline{\theta_{sim}}) + \overline{\theta_{obs}} \quad (1)$$

where θ_{sim} are the simulated soil moisture values, θ_{obs} is the ESA CCI soil moisture observations, $\sigma_{\theta_{sim}}$ and $\sigma_{\theta_{obs}}$ are the standard deviations of the simulated and observed soil moisture values and $\overline{\theta_{\mathrm{obs}}}$ and $\overline{\theta_{\mathrm{obs}}}$ are the means of the simulated and observed soil moisture values.

When comparing the original and the rescaled soil moisture, it is observed that the mean-standard deviation technique effectively removes the biases between the simulated and observed soil moisture time series (see Figure 1 of the Supplementary Information).

3.3 Calibration and validation strategy

Alternative single objective calibration approaches based on discharge, actual evapotranspiration and surface soil moisture and a multiobjective calibration approach based on actual evapotranspiration and surface soil moisture were inter-compared. Five different calibration scenarios were carried out. Calibration scenario S0 represents the reference calibration scenario, which was not locally calibrated for the Oum Er Rbia basin, but uses a-priori model parameters derived from vegetation, soil properties and geological information at a global scale (latest model version of PCR-GLOBWB). Calibration scenario S1 aims to calibrate the hydrological model using in-situ discharge observations, following the traditional calibration approach. Calibration scenarios S2 and S3 use GLEAM actual evapotranspiration and ESA CCI surface soil moisture time series for calibration, respectively. Calibration scenario S4 represents the multiobjective calibration approach and it consists of a step-wise calibration scheme that attempts to combine the strengths of calibration scenarios S2 and S3. Step one is simply scenario S2, where all the model parameters are allowed to be adjusted based on GLEAM actual evapotranspiration. In step two, those parameters that are clearly identified by calibration scenario S2 are held constant and the remaining parameters are allowed to be adjusted according to ESA CCI surface soil moisture, calibration scenario S3.

The five calibration scenarios were analysed for each of the three global precipitation products to study their impact on model parameters calibration and model performance. The calibration scenarios are described in Table 2, including the scenario identifier.

For the calibration using in-situ observed discharge time series (S1), two river gauge observation time series were used (section 3.2.2). The objective function to maximize for the calibration scenarios was Kling-Gupta efficiency (KGE) , instead of the traditional Mean Squared Error (MSE) or Nash Sutcliffe efficiency (NSE) to avoid underestimating the variability of values (Gupta et al., 2009). The mathematical formulation and description of the used objective function are included in section 3.4.

To calibrate PCR-GLOBWB for each of the three precipitation products, 81 runs with different parameter values were simulated: minimum soil water capacity (W_{min}), soil saturated hydraulic conductivites ($K_{\text{sat 1}}$, $K_{\text{sat 2}}$ and $K_{\text{sat 3}}$) and baseflow recession coefficient (J). These model parameters, which vary spatially over the basin, influence different model parts of the model behaviour, as it was explained in section 3.1. For the variation of the parameter values, spatially uniform prefactors were used: f_w, f_K and f_j (Table 3). The remaining model parameters were kept fixed.

The prefactors to vary model parameter values were referred to the parameters of the S0 calibration scenario. The spatial distribution of the parameters W_{min}, K_{sat} and J used in S0 scenario can be found in Figure A1 of Appendix A.

Furthermore, the uncertainty of reference potential evapotranspiration ($E_{p,0_{ref}}$) was also investigated using a correction prefactor, f_e, to this model variable. Considered values for f_e prefactor are included with the previously mentioned ones in Table 3.

As reference calibration scenario, S0 prefactors are: $f_w = 1$, $f_K = 0$, $f_j = 1$ and $f_e = 1$. The model performances of all the simulations were evaluated for each of the five calibration scenarios to identify the best prefactor sets as the calibrated prefactor sets.

All the simulations were performed at a daily temporal resolution for the 32-year period 1979-2010. The 2-year period 1979-1980 was used to spin up the hydrological model until reaching a dynamically steady state. The model was calibrated based on monthly values of discharge, actual evapotranspiration and surface soil moisture. Validation was also carried out at a monthly temporal resolution but exclusively for streamflow, aiming to analyse if similar discharge estimates may be obtained with a calibrated model based on remotely sensed observations (S2, S3 and S4), in comparison with a model traditionally calibrated to in-situ discharge data (S1). The 13-year period 1981-1993 was used for model calibration and during the 17-year period 1994-2010, the model was validated.

3.4 Performance metrics

To inter-compare the three global precipitation products six metrics were used: Nash-Sutcliffe efficiency (NSE), Kling-Gupta efficiency (KGE), Pearson's correlation coefficient (r) and Percent Bias ($PBias$). Moreover, one of those metrics, KGE, was chosen as objective function to calibrate and validate model performance for each calibration scenario. NSE, $PBias$ and r were also used as additional assessment measurements in the validation procedure.

Nash-Sutcliffe efficiency (Nash and Sutcliffe, 1970), NSE, is defined as

$$NSE = 1 - \frac{\sum_{t=1}^{n}[x(t) - y(t)]^2}{\sum_{t=1}^{n}[y(t) - \overline{y}]^2} \tag{2}$$

where $x(t)$ and $y(t)$ are the modeled and observed variable at t time step (months), $\overline{y}$ is the mean of observed data and n is the total number of observations. NSE is widely used for calibrating and validating hydrological models in terms of discharge. NSE varies from $-\infty$ to 1. If $NSE = 0$, modeled values perform as well as the mean of the observations. If $NSE < 0$, modeled values perform worse than the mean of the observations.

Gupta et al. (2009) analysed various decompositions of NSE and proposed an alternative model performance criteria, Kling-Gupta efficiency (KGE), to avoid the problems that can be derived of using the NSE criterion (e.g. high sensitivity to extreme values and bias). KGE is given as

$$KGE = 1 - \sqrt{(r-1)^2 + (\alpha - 1)^2 + (\beta - 1)^2} \tag{3}$$

where r represents the Pearson's correlation coefficient, α is the ratio between the variance of the modeled variable and the variance of the observed variable and β is the ratio between the mean of the modeled variable and the mean of the observed variable, i.e. β represents the bias. Analogous to NSE, KGE ranges from $-\infty$ to 1 with an ideal value of 1. KGE measures simultaneously bias, variability and correlation.

Pearson's correlation coefficient (Pearson, 1896), r, measures the degree of linear association between modeled and observed values and it is defined as

$$r = \frac{\sum_{t=1}^{n}(x(t) - \overline{x})(y(t) - \overline{y})}{\sqrt{\sum_{t=1}^{n}(x(t) - \overline{x})^2}\sqrt{\sum_{t=1}^{n}(y(t) - \overline{y})^2}} \tag{4}$$

where $x(t)$ and $y(t)$ are the modeled and observed variable at t time step (months), $\overline{y}$ is the mean of observed data, $\overline{x}$ is the mean of modeled data and n is the total number of observations. r varies within the interval [-1,1]. r is mainly used in hydrological modeling to evaluate the timing of modeled to observed time series.

Percent Bias indicates the average tendency of the modeled values to over- or underestimate the observations. $PBias$, is calculated in percentage terms as

$$PBias = 100 \times \frac{\sum_{t=1}^{n}(x(t) - y(t))}{\sum_{t=1}^{n} y(t)} \tag{5}$$

The optimal value of $PBias$ is 0.

When the performance metrics were calculated between simulated and observed soil moisture estimates, the subscript $_{sm}$ was added to the metric, i.e. NSE_{sm}, KGE_{sm}, r_{sm} and $PBias_{sm}$. Similarly, when comparing actual evapotranspiration estimates, precipitation and discharge, the added subscripts were $_{evap}$, $_{precip}$ and $_{q}$, respectively.

4 Results

4.1 Inter-comparison of precipitation products

To inter-compare the precipitation products, the annual mean precipitation for the study time period (1979-2010) for each forcing dataset was calculated (Figures 3a, 3b and 3c). In addition to the spatial resolution difference, MSWEP was able to capture the rainfall pattern over the Atlas Mountains rather well, which was only roughly distinguished by WFDEI and unrecognized by EI. The finer spatial resolution and the combination of reanalysis, satellite and in-situ data are probably the reasons for its more plausible spatial pattern. Furthermore, climatology of precipitation products was analyzed (Figure 3d). WFDEI ranged from 4.5 mm in July to 57 mm in February, whereas EI and MSWEP showed a lesser variability with precipitation values from 10.5 mm in July to 42.6 mm in November. Smaller differences between WFDEI and EI and MSWEP were observed during the summer months. EI and MSWEP showed similar temporal precipitation patterns. Annual mean precipitation over the entire basin obtained with MSWEP (355.15 mm) was approximately 80 mm higher than with EI (276.67 mm). Similar annual median values were obtained with the three global precipitation products, although the distribution of WFDEI highly differed from the other two products.

Moreover, various performance metrics between the interpolated and in-situ ground data were calculated and shown in Figure 4. Overall, EI and MSWEP provided a better fit to the station data compared to WFDEI, with higher KGE_{precip}, NSE_{precip} and r_{precip} than WFDEI. When comparing EI with MSWEP, similar values of KGE_{precip} and NSE_{precip} were found, whereas higher differences existed in r_{precip} and $PBias_{precip}$. In terms of correlation MSWEP showed the best performance, but EI showed the lowest Percent Bias at both weather stations, with a value of less than 10 %. Only two weather stations were found within the basin for the previous analysis. These measurements were considered too scarce to cover the basin and to discard

the precipitation product with the lowest performance (WFDEI). Therefore, the three global precipitation products were used to calibrate PCR-GLOBWB under the five calibration scenarios.

4.2 Calibration results

Model parameters were calibrated using discharge, evapotranspiration and soil moisture observations through five different calibration scenarios for the time period 1981-1993. Figure 5 shows results of all runs produced in this study for different calibration scenarios based on: in-situ discharge observations (S1) at Ait Ouchene (Figure 5a) and Mechra Eddahk (Figure 5b), GLEAM actual evapotranspiration (S2, Figure 5c) and ESACCI surface soil moisture (S3, Figure 5d). For each sub-figure in Figure 5, KGE results (y-axis) of using the three precipitation products were plotted in different rows (top: EI, middle: WFDEI and bottom: MSWEP) and prefactor values were plotted in different columns (x-axis, 1^{st} column: f_e, 2^{nd} column: f_j, 3^{rd} column: f_k and 4^{th} column: f_w). Each scatterplot contains 81 dots representing each run with a different combination of parameter values. This means that the KGE values are the same in the four scatterplots of a row (y- axis), but in each of these scatterplots, they were plotted against a different prefactor (x-axis). With Figure 5, prefactor, and therefore parameter, ranges leading to better and worse performances could be distinguished, as well as their global optimal values. If no optimal value could be inferred, prefactors from the calibration scenario S0 were maintained ($f_e = 1$, $f_j = 0$, $f_k = 0$ and $f_w = 1$).

Once the best runs for each calibration scenario were identified, their discharge performance was checked at the two gauging stations: Mechra Eddahk, in Figure 6, and Ait Ouchene, in Figure 2 of the Supplementary Information. Observed discharge (y-axis) and estimated discharge (x-axis) were plotted in Figure 6 for the five calibration scenarios. Different rows in Figure 6 indicate the three global precipitation products (top: EI, middle: WFDEI and bottom: MSWEP) and different columns indicate the five calibration scenarios (1^{st} column: S0, 2^{nd} column: S1, 3^{rd} column: S2, 4^{th} column: S3 and 5^{th} column: S4). The performance indicators NSE and KGE for discharge were included in every scatterplot in Figure 6 (NSE_q and KGE_q).

To summarize results shown in Figures 5 and 6, Table 4 includes for each calibration scenario the identified optimal parameters values and the KGE_q performance values at Ait Ouchene and Mechra Eddahk.

4.2.1 Calibration using in-situ observed discharge time series (S1)

Figures 5a and 5b (calibration scenario S1) are similar. From these figures, f_e (1^{st} column) and f_w (4^{th} column) were well identified by discharge calibration at both gauging stations when forced with any of the three precipitation products. $f_e = 1.25$ and $f_w = 1.25$ led to the highest KGE_q values. However, it was not possible to identify the best prefactors of f_j (2^{nd} column) and f_k (3^{rd} column). There were no clear and distinct maximum values in the scatterplots of these figures, hence $f_j = 0$ and $f_k = 0$ were used.

From Figure 6 (2^{nd} column), the highest discharge performance was obtained when the model was calibrated with in-situ discharge observations (S1).

For all the calibration scenarios, a few general observations could be made. Scatterplots (Figure 6) highlighted an overall better agreement and a lower bias between discharge observations and estimates for the Ait Ouchene (see Figure 2 in the Supplementary Information) than for Mechra Eddahk station. KGE_q values at Ait Ouchene station for calibration scenario S0 were lower than for Mechra Eddahk station. This may be due to their different locations within the basin, the former one being situated in the Atlas Mountains, where precipitation estimates can be less accurate, and in a tributary of the Oum Er Rbia River, whose representation in PCR-GLOBWB can be limited by the model spatial resolution.

Scatterplots (Figure 6) also showed that estimated discharges were closer to observed discharges at both gauging stations when PCR-GLOBWB was forced with EI precipitation. Moreover, scatterplots indicated a worse agreement and a tendency to overestimate discharge when WFDEI and MSWEP were used. KGE_q values for the reference calibration scenario S0 at Mechra Eddahk were 0.607, 0.325 and 0.561 when EI, WFDEI and MSWEP were used as forcing data respectively. These performance discrepancies were related with the differences between EI, WFDEI and MSWEP precipitation products discussed in section 4.1. The lower quality of WFDEI in this region compared with the other precipitation datasets may be a possible reason of the lower discharge performance. When MSWEP was compared with in-situ precipitation data, performance in terms of correlation was higher than EI. However, EI showed less bias. The higher performance of discharge estimates when PCR-GLOBWB was forced with EI may be due to this bias difference and that the validation was carried out at a monthly temporal resolution, reducing the impact of correlation.

4.2.2 Calibration using GLEAM actual evapotranspiration time series (S2)

Figure 5c (calibration scenario S2) indicated that only prefactor f_e (1^{st} column) could be clearly identified (the highest KGE_{evap} values were obtained with $f_e = 1.25$), whereas the remainder of the prefactors (f_j, f_w and f_k) were non identifiable, suggesting that evapotranspiration-based calibration may be unreliable in their identification. Therefore, model run with prefactors $f_e = 1.25$, $f_j = 0$, $f_k = 0$ and $f_w = 1$ was considered as the calibrated run based on the evapotranspiration performance.

From Figure 6 (3^{rd} column), results indicated an increase of KGE_q and NSE_q values when GLEAM evapotranspiration was used for model calibration compared to the reference scenario (S0, 1^{st} column of Figure 6). However, higher model performance values were obtained when calibrating based on in-situ discharge observations (S1, 2^{nd} column of Figure 6).

4.2.3 Calibration using ESA CCI surface soil moisture time series (S3)

Figure 5d (calibration scenario S3) indicated that prefactors f_k (3^{rd} column) and f_w (4^{th} column) could be identified, $f_w = 1.25$ and $f_k = 0.25$. There was a clear maximum value of KGE_{sm} with these prefactors values. Prefactors f_e (1^{st} column) and f_j (2^{nd} column) were not identifiable when soil moisture was used for calibration. Therefrom, the calibrated run based on soil moisture performance was the model run with prefactors $f_e = 1$, $f_j = 0$,$f_k = 0.25$ and $f_w = 1.25$. This implies that ESA CCI soil moisture may be used to indirectly tune groundwater recharge by calibrating the upper soil saturated hydraulic conductivities, K_{sat}.

From Figure 6 (4^{th} column), scatterplots indicated an improvement in the correspondence between observed and estimated discharge compared to the non-calibrated scenario (S0, 1^{st} column of Figure 6). Similarly to calibration scenario S2 (3^{rd} column of Figure 6), this improvement was lower than when the model was calibrated based on ground discharge observations (S1, 2^{nd} column of Figure 6).

The calibrated runs based on evapotranspiration (S2, 3^{rd} column of Figure 6) and soil moisture (S3, 4^{th} column of Figure 6) resulted in lower discharge performances compared to the reference scenario (S0) at some cases, e.g. when EI precipitation was used at Mechra Eddahk location, $KGE_q(S0) = 0.607$, $KGE_q(S2) = 0.534$ and $KGE_q(S3) = 0.522$.

4.2.4 Step-wise calibration using GLEAM actual evapotranspiration and ESA CCI surface soil moisture time series (S4)

Calibration scenario S4 attempted to combine the strengths of scenarios S2 and S3. In the first step, the model was calibrated using GLEAM evapotranspiration (S2, Figure 5c). From Figure 5c, only f_e prefactor was well identified (the highest KGE_{evap} value was obtained with $f_e = 1.25$). In the second step, f_e prefactor that had been identified was held constant and the remaining three prefactors were allowed to be calibrated according to ESA CCI soil moisture (S3, Figure 5d). From Figure 5d, f_w and f_k were identifiable (the highest KGE_{sm} values were obtained with $f_w = 1.25$ and $f_k = 0.25$). As a result, for calibration scenario S4, the prefactors identified during the evapotranspiration calibration (S2): $f_e = 1.25$ and during the soil moisture calibration (S3): $f_w = 1.25$ and $f_k = 0.25$ were adopted. This step-wise calibration approach using multiple system variables allowed to identify more parameters than when those variables were separately used. Nonetheless, neither of the steps in calibration scenario S4 allowed the clear identification of f_j, so its value for the calibration scenario S0 was used, $f_j = 0$.

From Figure 6 (5^{th} column), calibration using GLEAM evapotranspiration and ESA CCI soil moisture led to further improvements than when these observations were separately used. For example, when MSWEP precipitation was used to model discharge at Mechra Eddahk station, KGE_q varied between 0.703, 0.693, 0.613 and 0.573 for calibration scenarios S1, S4, S2 and S3, respectively ($KGE_q = 0.561$ for the reference scenario S0). At Ait Ouchene station (see Figure 2 in the Supplementary Information), KGE_q varied between 0.520, 0.342, 0.331 and 0.271 for calibration scenarios S1, S4, S2 and S3, respectively ($KGE_q = -0.542$ for the reference scenario S0).

4.3 Validation results

Once the model had been calibrated for each calibration scenario and each precipitation product, comparisons between estimates (before and after the calibration) and observations of actual evapotranspiration, surface soil moisture and discharge were carried out for the validation time period (1994-2011). To perform the analysis of these results, time series plots were included in Figures 7 and 8.

In Figure 7a, simulated actual evapotranspiration time series of the reference run (S0, red dashed line) and the step-wise calibrated run (S4, purple dashed line) were plotted against GLEAM actual evapotranspiration observations (black line). Similarly as Figure 7a, Figure 7b shows simulated surface soil moisture of the reference run (S0, red dashed line) and the step-wise

calibrated run (S4, purple dashed line) plotted against ESA CCI surface soil moisture time series (black line). The rescaled soil moisture time series (after mean-standard deviation matching technique applied, see section 3.2.4) are shown. In Figure 7c, estimated discharge of the reference run (S0, red dashed line) and the step-wise calibrated run (S4, purple dashed line) were plotted against discharge observations (black line) at Mechra Eddahk. KGE values for actual evapotranspiration, surface soil moisture and discharge were included in Figures 7a, 7b and 7c. For the sake of simplicity, only results when the model was forced with MSWEP precipitation are shown.

Similarly to Figure 7, Figure 8 shows simulated evapotranspiration (Figure 8a), surface soil moisture (Figure 8b) and discharge (Figure 8c) against observations. However, in Figure 8, estimates of the discharge-calibrated run (S1, red dashed line) and the step-wise calibrated run (S4, purple dashed line) were plotted against observations (black line). With Figure 8, the impact on calibration of using in-situ discharge and remotely sensed evapotranspiration and soil moisture observations could be compared.

Reference run (S0) provided evapotranspiration (Figure 7a) and soil moisture (Figure 7b) estimates fairly close to observations with $KGE_{evap} = 0.586$ and $KGE_{sm} = 0.828$. Discharge estimates of calibration scenario S0 performed well at Mechra Eddahk (Figure 7c). Discharge performance of the reference run (S0) was lower at Ait Ouchene. From Figure 7a, the calibration procedure based on GLEAM evapotranspiration and ESA CCI soil moisture (S4) produced an increase of 18 % in KGE_{evap} compared to the reference run (S0). From Figure 7b, estimated and observed surface soil moisture time series showed a good correspondence. KGE_{sm} difference of 0.028 was found between the reference (S0) and the step-wise (S4) calibration scenarios. From Figure 7c, the step-wise calibrated run (S4) reproduced the monthly observed discharge well, except some simulated extreme peaks which were not observed, e.g. January and June in 2002 and some which were not simulated properly, e. g. January and May in 1996 and 1997. This lack of fit may be due to errors in the precipitation data, because higher discharge differences were shown when WFDEI and MSWEP products were used in comparison to EI product. Other possible reasons may be related with model structural deficiencies. When comparing discharge time series (Figure 7c), calibration scenario S4 slightly improved KGE_q compared to calibration scenario S0, with KGE_q values varying from 0.648 to 0.710.

From Figure 8a, an increase of 14 % in KGE_{evap} was produced when the discharge calibration scenario (S1) was used compared to the reference run (S0). This improvement in evapotranspiration estimates was higher when calibrating the model using GLEAM evapotranspiration and ESA CCI soil moisture (S4, $KGE_{evap} = 0.689$) than when calibrating it only for ground discharge (S1, $KGE_{evap} = 0.666$). Similarly to Figure 8a showing the evapotranspiration comparison, Figure 8b indicated that a higher KGE_{sm} value was obtained when using GLEAM and ESA CCI observations for calibration (S4, $KGE_{sm} = 0.856$) than when calibration was based on in-situ discharge observations (S1, $KGE_{sm} = 0.834$). From Figure 8c comparing discharge time series at Mechra Eddahk, step-wise calibration scenario S4 led to an increase of 10 % in KGE_q, compared to the increase of 5 % obtained when discharge observations were used for calibration (S1). However, at Ait Ouchene the discharge performance improvement was lower when evapotranspiration and soil moisture observations (S4) were used for calibration than when in-situ discharge measurements were used (S1). This may be due to the lower performance of the reference run (S0) at Ait Ouchene. To compare

To further understand the added value of using GLEAM evapotranspiration and ESA CCI soil moisture data for model calibration and inter-compare the impact of the calibration scenarios, the variations of KGE_q, NSE_q, r_q and $PBias_q$ between each calibration scenario (S1, S2, S3 and S4) and the reference calibration scenario (S0) were calculated and plotted for the validation time period in Figure 9. Rows indicate the three global precipitation products and columns indicate the performance indicators. The variations of the performance metrics are shown with barplots for the two gauging stations, Ait Ouchene and Mechra Eddahk. At each location, a positive value of KGE_q, NSE_q, $PBias_q$ and r_q means that either S1, S2, S3 or S4 scenario obtained a higher skill score than S0, whereas a negative value means that those scores decreased after calibration.

Figure 9 showed that variations of the performance indicators were lower when EI precipitation product was used. The highest differences between the calibration scenarios were obtained when the model was forced with WFDEI precipitation. In the inter-comparison of the calibration scenarios, calibration scenario using in-situ observed discharge data (S1) obtained overall the highest increase of KGE_q,NSE_q and r_q and the highest reduction of $PBias_q$ when any of the precipitation products were used, as it was expected. Similar KGE_q and NSE_q increases and $PBias_q$ decreases were obtained when the model was calibrated using only soil moisture (S3) and using the combination of evapotranspiration and soil moisture (S4), but larger improvements in r_q were obtained with the step-wise calibration scenario (S4). KGE_q, NSE_q and r_q gains when comparing calibration scenarios S2 and S0 were positive, but of a lower magnitude than when model was calibrated in scenarios S3 and S4. The higher performance of scenario S4 may be due to the fact that this calibration approach used multiple system variables providing more hydrological information and allowing the identification of more parameters than when those variables were separately used.

In each barplot of Figure 9, metrics improvements were larger at Ait Ouchene station than at Mechra Eddahk station. This is due to the lower discharge performance for the reference calibration scenario S0 at the former gauging location. Note that in some cases where the change in KGE_q was negative (e.g. when EI precipitation was used at Ait Ouchene station), this is because although there was an improvement in the KGE_q performance indicator during the calibration time period, when calculating it for the validation time period, it is possible that the metric slightly worsens. Note that some variations in NSE_q, $PBias_q$ and r_q were small or close to 0, because its calibration was optimised for KGE_q and not for those particular metrics in terms of discharge. A possible route to overcome this problem may be to use various performance indicators (for example, KGE, NSE, $PBias$ and r) as objective functions to optimize in each calibration scenario, instead of using a single one. This multiobjective calibration approach may further improve discharge model estimates.

5 Discussion and conclusions

This study investigated alternative routes to calibrate the large-scale hydrological model PCR-GLOBWB using earth observations globally available for the data-poor river basin of Oum Er Rbia in Morocco. Three global precipitation products, EI, WFDEI and MSWEP, were inter-compared and applied to force PCR-GLOBWB. Five different calibration scenarios were followed where GLEAM actual evapotranspiration and ESA CCI surface soil moisture data were used to identify model pa-

rameters with the aim to improve discharge estimates. In-situ discharge observations were also used for calibration, as they are traditionally used to calibrate hydrological models.

Results showed that GLEAM actual evapotranspiration and ESA CCI soil moisture observations may be used to calibrate determined PCR-GLOBWB model parameters. GLEAM actual evapotranspiration was used to calibrate the reference potential evapotranspiration (f_e) as expected, affecting the water exchange between the top soil layer and the atmosphere and hence the soil water balance. ESA CCI soil moisture data was used to calibrate the minimum soil water capacity (f_w) and the saturated hydraulic conductivities of the soil layers (f_k), determining the surface runoff generation response, the shallow sub-surface flow and the groundwater recharge. However, calibration using only GLEAM evapotranspiration data or only ESA CCI soil moisture can result in more than one parameters combination to be optimal in terms of discharge (overparametrization or equifinality problem). To overcome this problem, a step-wise calibration scenario based on both observations, evapotranspiration and soil moisture, was necessary to identify the optimal values of reference potential evapotranspiration (f_e), runoff-infiltration partitioning parameters (f_w) and the soil saturated hydraulic conductivity (f_k). Nonetheless, neither of these observations was used to calibrate the baseflow from the active groundwater layer (f_j). To identify baseflow recession coefficient parameter (f_j) a multiobjective calibration approach to streamflow observations could be followed. Similarly to Fenicia et al. (2007), multiple objective functions may be optimized in sequential steps for high flows, low flows and timing.

Spatially uniform prefactors for the entire Oum Er Rbia basin were used for the variation of the parameter values in this study. Developing novel calibration strategies where prefactors and so, model parameters vary with soil type, land use, elevation and/or other characteristics within the basin would be a promising research route to investigate. Furthermore, the present work inter-compares five calibration scenarios using a brute force method, where several combinations of parameters values were tested and the best performing was selected. For these combinations, and due to computational limitations, only four prefactors were considered leading to 81 model runs per precipitation product. Using more prefactor values and therefore, more runs may improve the estimation of the optimal parameters set for each calibration scenario. A suggestion for future studies may be to use an Ensemble Kalman Filter to calibrate the hydrological model, as previously presented in literature (Moradkhani et al., 2005; Wanders et al., 2014). Furthermore, the validation of this study was carried out exclusively on streamflow. Other validation approaches, including the empirical orthogonal functions, wavelet analysis or their combination, may be another promising way towards a more in-depth validation of distributed hydrological models (Mascaro et al., 2015; Koch et al., 2015; Fang et al., 2015).

A step-wise calibration approach based on GLEAM actual evapotranspiration and ESA CCI soil moisture resulted in discharge estimates of acceptable accuracy (Moriasi et al., 2007), compared to discharge estimates derived from a model that was calibrated to in-situ discharge measurements. Traditional calibration to in-situ discharge measurements resulted in the highest model performance. A model calibrated only on evapotranspiration or soil moisture observations achieved a lower discharge performance than when they were used together.

In the inter-comparison between the three global precipitation products, WFDEI showed the lowest performance, whereas EI and MSWEP performed quite well. Apart from the in-situ discharge calibration scenario, the highest discharge improvement

was obtained when the two latter forcing data were used in combination with a step-wise calibration approach based on evapotranspiration and soil moisture observations.

Results indicated that precipitation impact on streamflow estimates was more significant than the one derived from calibrating model parameters, thus the lower quality of WFDEI compared to EI and MSWEP, decreased model performance and calibration was biased in order to compensate precipitation errors. Further investigation of the effect of precipitation errors on model efficiency, but also on model parameters estimation may be an interesting route for hydrological research (Andréassian et al., 2004; Looper et al., 2012).

Although there is still room for further research, this study showed that globally available earth observations, such as evapotranspiration or soil moisture, can be used to further parameterize large-scale hydrological models providing reasonable discharge estimates at regional or basin scale. In principle, these calibration approaches can be applied and investigated in other basins without or with limited in-situ ground hydro-meteorological data (ungauged basins), not only to estimate discharge, but also to improve the understanding of the hydrological processes in the basin. Results suggested the potential of using other satellite products for hydrological modeling studies, including soil moisture products such as AMSR-E (Njoku et al., 2003) and SMOS (Kerr et al., 2001), evapotranspiration products such as SEBAL (Bastiaanssen et al., 1998) and MOD16 (Nishida, 2003), total water storage products such as GRACE (Tapley et al., 2004), etc. The spatial information of these satellite-based products could be used in a different way than the one explained in this study. For example, a calibration scenario based on a pixel by pixel, instead of basin average, comparison of surface soil moisture and actual evapotranspiration model estimates and observations could further improve discharge estimates. This calibration approach would have to take into account the spatial variability of the variables over the basin. Previous studies investigate how to incorporate spatial information into hydrological models using innovative spatial performance metrics to analyse the spatial sensitivity of simulated land-surface patterns (Koch et al., 2017).

Future studies may investigate step-wise calibration approaches using the combined information from multiple hydrological system variables. By incorporating several data products, different parts or components of the model can be optimized to increase the overall model performance. Another approach could be to calibrate the model to different variables with multiple objective functions - multiobjective calibration- (Gupta et al., 1998; Khu and Madsen, 2005; Fenicia et al., 2007). Alternatively, these hydro-meteorological data which are globally available may be used to identify and develop relationships between different basins using similarities, classification and scaling frameworks, as presented in previous studies (Samaniego et al., 2010b; Kumar et al., 2013).

References

Anderson, R. M., Koren, V. I., and Reed, S. M.: Using SSURGO data to improve Sacramento Model a priori parameter estimates, Journal of Hydrology, 320, 103–116, 2006.

Andréassian, V., Perrin, C., and Michel, C.: Impact of imperfect potential evapotranspiration knowledge on the efficiency and parameters of watershed models, Journal of Hydrology, 286, 19–35, 2004.

Bastiaanssen, W., Menenti, M., Feddes, R., and Holtslag, A.: A remote sensing surface energy balance algorithm for land (SEBAL). 1. Formulation, Journal of hydrology, 212, 198–212, 1998.

Beck, H. E., de Jeu, R. A., Schellekens, J., van Dijk, A. I., and Bruijnzeel, L. A.: Improving curve number based storm runoff estimates using soil moisture proxies, IEEE Journal of selected topics in applied earth observations and remote sensing, 2, 250–259, 2009.

Beck, H. E., van Dijk, A. I., de Roo, A., Miralles, D. G., McVicar, T. R., Schellekens, J., and Bruijnzeel, L. A.: Global-scale regionalization of hydrologic model parameters, Water Resources Research, 2016a.

Beck, H. E., van Dijk, A. I., Levizzani, V., Schellekens, J., Miralles, D. G., Martens, B., and de Roo, A.: MSWEP: 3-hourly 0.25 global gridded precipitation (1979–2015) by merging gauge, satellite, and reanalysis data, Hydrology and Earth System Sciences, 2016b.

Bouchaou, L., Michelot, J., Qurtobi, M., Zine, N., Gaye, C., Aggarwal, P., Marah, H., Zerouali, A., Taleb, H., and Vengosh, A.: Origin and residence time of groundwater in the Tadla basin (Morocco) using multiple isotopic and geochemical tools, Journal of hydrology, 379, 323–338, 2009.

Brocca, L., Moramarco, T., Melone, F., Wagner, W., Hasenauer, S., and Hahn, S.: Assimilation of surface-and root-zone ASCAT soil moisture products into rainfall–runoff modeling, IEEE Transactions on Geoscience and Remote Sensing, 50, 2542–2555, 2012.

Budyko, M.: Climate and Life, 508 pp, 1974.

Campo, L., Caparrini, F., and Castelli, F.: Use of multi-platform, multi-temporal remote-sensing data for calibration of a distributed hydrological model: an application in the Arno basin, Italy, Hydrological processes, 20, 2693–2712, 2006.

Cheng, L., Yaeger, M., Viglione, A., Coopersmith, E., Ye, S., and Sivapalan, M.: Exploring the physical controls of regional patterns of flow duration curves–Part 1: Insights from statistical analyses, Hydrology and Earth System Sciences, 16, 4435–4446, 2012.

Dee, D., Uppala, S., Simmons, A., Berrisford, P., Poli, P., Kobayashi, S., Andrae, U., Balmaseda, M., Balsamo, G., Bauer, P., et al.: The ERA-Interim reanalysis: Configuration and performance of the data assimilation system, Quarterly Journal of the royal meteorological society, 137, 553–597, 2011.

Dorigo, W., Gruber, A., De Jeu, R., Wagner, W., Stacke, T., Loew, A., Albergel, C., Brocca, L., Chung, D., Parinussa, R., et al.: Evaluation of the ESA CCI soil moisture product using ground-based observations, Remote Sensing of Environment, 162, 380–395, 2015.

Dornes, P. F., Tolson, B. A., Davison, B., Pietroniro, A., Pomeroy, J. W., and Marsh, P.: Regionalisation of land surface hydrological model parameters in subarctic and arctic environments, Physics and Chemistry of the Earth, Parts A/B/C, 33, 1081–1089, 2008.

Fang, X., Pomeroy, J., Westbrook, C., Guo, X., Minke, A., and Brown, T.: Prediction of snowmelt derived streamflow in a wetland dominated prairie basin, Hydrology and Earth System Sciences, 14, 991–1006, 2010.

Fang, Z., Bogena, H., Kollet, S., Koch, J., and Vereecken, H.: Spatio-temporal validation of long-term 3D hydrological simulations of a forested catchment using empirical orthogonal functions and wavelet coherence analysis, Journal of hydrology, 529, 1754–1767, 2015.

Fenicia, F., Savenije, H. H., Matgen, P., and Pfister, L.: A comparison of alternative multiobjective calibration strategies for hydrological modeling, Water Resources Research, 43, 2007.

Gupta, H. V., Sorooshian, S., and Yapo, P. O.: Toward improved calibration of hydrologic models: Multiple and noncommensurable measures of information, Water Resources Research, 34, 751–763, 1998.

Gupta, H. V., Wagener, T., and Liu, Y.: Reconciling theory with observations: elements of a diagnostic approach to model evaluation, Hydrological Processes, 22, 3802–3813, 2008.

Gupta, H. V., Kling, H., Yilmaz, K. K., and Martinez, G. F.: Decomposition of the mean squared error and NSE performance criteria: Implications for improving hydrological modelling, Journal of Hydrology, 377, 80–91, 2009.

Hafeez, M., van de Giesen, N., Bardsley, E., Seyler, F., Pail, R., and Taniguchi, M.: GRACE, remote sensing and ground-based methods in multi-scale hydrology: proceedings of symposium J-HO1 held during IUGG2011, IAHS Publications, 2011.

Hagemann, S. and Gates, L. D.: Improving a subgrid runoff parameterization scheme for climate models by the use of high resolution data derived from satellite observations, Climate Dynamics, 21, 349–359, 2003.

Houdret, A.: Les conflits autour de l'eau au Maroc: origines sociopolitiques et écologiques et perspectives pour transformation des conflits, 2008.

Hrachowitz, M., Savenije, H., Blöschl, G., McDonnell, J., Sivapalan, M., Pomeroy, J., Arheimer, B., Blume, T., Clark, M., Ehret, U., et al.: A decade of Predictions in Ungauged Basins (PUB)—a review, Hydrological sciences journal, 58, 1198–1255, 2013.

Huffman, G. J., Bolvin, D. T., Nelkin, E. J., Wolff, D. B., Adler, R. F., Gu, G., Hong, Y., Bowman, K. P., and Stocker, E. F.: The TRMM multisatellite precipitation analysis (TMPA): Quasi-global, multiyear, combined-sensor precipitation estimates at fine scales, Journal of Hydrometeorology, 8, 38–55, 2007.

Immerzeel, W. and Droogers, P.: Calibration of a distributed hydrological model based on satellite evapotranspiration, Journal of Hydrology, 349, 411–424, 2008.

Immerzeel, W. W., Droogers, P., De Jong, S., and Bierkens, M.: Large-scale monitoring of snow cover and runoff simulation in Himalayan river basins using remote sensing, Remote sensing of Environment, 113, 40–49, 2009.

Isenstein, E. M., Wi, S., Yang, Y. E., and Brown, C.: Calibration of a distributed hydrologic model using streamflow and remote sensing snow data, in: World Environmental and Water Resources Congress 2015, pp. 973–982, ASCE, 2015.

Jacobs, J. M., Myers, D. A., and Whitfield, B. M.: Improved rainfall/runoff estimates using remotely sensed soil moisture, JAWRA Journal of the American Water Resources Association, 39, 313–324, 2003.

Jones, A., Breuning-Madsen, H., Brossard, M., Dampha, A., Deckers, J., Dewitte, O., Gallali, T., Hallett, S., Jones, R., Kilasara, M., et al.: Soil atlas of Africa, European Commission, 2013.

Joyce, R. J., Janowiak, J. E., Arkin, P. A., and Xie, P.: CMORPH: A method that produces global precipitation estimates from passive microwave and infrared data at high spatial and temporal resolution, Journal of Hydrometeorology, 5, 487–503, 2004.

Kerr, Y. H., Waldteufel, P., Wigneron, J.-P., Martinuzzi, J., Font, J., and Berger, M.: Soil moisture retrieval from space: The Soil Moisture and Ocean Salinity (SMOS) mission, IEEE transactions on Geoscience and remote sensing, 39, 1729–1735, 2001.

Khu, S. T. and Madsen, H.: Multiobjective calibration with Pareto preference ordering: An application to rainfall-runoff model calibration, Water Resources Research, 41, 2005.

Kite, G. and Droogers, P.: Comparing evapotranspiration estimates from satellites, hydrological models and field data, Journal of Hydrology, 229, 3–18, 2000.

Koch, J., Jensen, K. H., and Stisen, S.: Toward a true spatial model evaluation in distributed hydrological modeling: Kappa statistics, Fuzzy theory, and EOF-analysis benchmarked by the human perception and evaluated against a modeling case study, Water Resources Research, 51, 1225–1246, 2015.

Koch, J., Mendiguren, G., Mariethoz, G., and Stisen, S.: Spatial sensitivity analysis of simulated land-surface patterns in a catchment model using a set of innovative spatial performance metrics., Journal of Hydrometeorology, 2017.

Kumar, R., Samaniego, L., and Attinger, S.: Implications of distributed hydrologic model parameterization on water fluxes at multiple scales and locations, Water Resources Research, 49, 360–379, 2013.

Liu, Y., Dorigo, W. A., Parinussa, R., de Jeu, R. A., Wagner, W., McCabe, M. F., Evans, J., and Van Dijk, A.: Trend-preserving blending of passive and active microwave soil moisture retrievals, Remote Sensing of Environment, 123, 280–297, 2012.

Liu, Y. Y., Parinussa, R., Dorigo, W. A., De Jeu, R. A., Wagner, W., Van Dijk, A., McCabe, M. F., and Evans, J.: Developing an improved soil moisture dataset by blending passive and active microwave satellite-based retrievals, Hydrology and Earth System Sciences, 15, 425–436, 2011.

Lo, M.-H., Famiglietti, J. S., Yeh, P.-F., and Syed, T.: Improving parameter estimation and water table depth simulation in a land surface model using GRACE water storage and estimated base flow data, Water Resources Research, 46, 2010.

Looper, J. P., Vieux, B. E., and Moreno, M. A.: Assessing the impacts of precipitation bias on distributed hydrologic model calibration and prediction accuracy, Journal of Hydrology, 418, 110–122, 2012.

López López, P., Wanders, N., Schellekens, J., Renzullo, L. J., Sutanudjaja, E. H., and Bierkens, M. F. P.: Improved large-scale hydrological modelling through the assimilation of streamflow and downscaled satellite soil moisture observations, doi:10.5194/hess-20-3059-2016, 2016.

Loukas, A. and Vasiliades, L.: Streamflow simulation methods for ungauged and poorly gauged watersheds, Natural Hazards and Earth System Sciences, 14, 1641–1661, 2014.

Martens, B., Miralles, D., Lievens, H., Fernández-Prieto, D., and Verhoest, N.: Improving terrestrial evaporation estimates over continental Australia through assimilation of SMOS soil moisture, International Journal of Applied Earth Observation and Geoinformation, 48, 146–162, 2016a.

Martens, B., Miralles, D., Lievens, H., van der Schalie, R., de Jeu, R., Fernández-Prieto, D., and Verhoest, N.: GLEAM v3: updated land evaporation and root-zone soil moisture datasets, in: EGU General Assembly Conference Abstracts, vol. 18, p. 4253, 2016b.

Mascaro, G., Vivoni, E. R., and Méndez-Barroso, L. A.: Hyperresolution hydrologic modeling in a regional watershed and its interpretation using empirical orthogonal functions, Advances in Water Resources, 83, 190–206, 2015.

Masih, I., Uhlenbrook, S., Maskey, S., and Ahmad, M.: Regionalization of a conceptual rainfall–runoff model based on similarity of the flow duration curve: A case study from the semi-arid Karkheh basin, Iran, Journal of hydrology, 391, 188–201, 2010.

Miralles, D., De Jeu, R., Gash, J., Holmes, T., and Dolman, A.: An application of GLEAM to estimating global evaporation, Hydrology and Earth System Sciences Discussions, 8, 1–27, 2011a.

Miralles, D., Holmes, T., De Jeu, R., Gash, J., Meesters, A., and Dolman, A.: Global land-surface evaporation estimated from satellite-based observations, Hydrology and Earth System Sciences, 15, 453–469, 2011b.

Moradkhani, H., Sorooshian, S., Gupta, H. V., and Houser, P. R.: Dual state–parameter estimation of hydrological models using ensemble Kalman filter, Advances in Water Resources, 28, 135–147, 2005.

Moriasi, D. N., Arnold, J. G., Van Liew, M. W., Bingner, R. L., Harmel, R. D., and Veith, T. L.: Model evaluation guidelines for systematic quantification of accuracy in watershed simulations, Transactions of the ASABE, 50, 885–900, 2007.

Mu, Q., Zhao, M., and Running, S. W.: Improvements to a MODIS global terrestrial evapotranspiration algorithm, Remote Sensing of Environment, 115, 1781–1800, 2011.

Nash, J. E. and Sutcliffe, J. V.: River flow forecasting through conceptual models part I—A discussion of principles, Journal of hydrology, 10, 282–290, 1970.

New, M., Lister, D., Hulme, M., and Makin, I.: A high-resolution data set of surface climate over global land areas, Climate research, 21, 1–25, 2002.

Nishida, K.: Validation of prototype MODIS evapotranspiration (MOD16) in the eastern Asia, in: AGU Fall Meeting Abstracts, 2003.

Njoku, E. G., Jackson, T. J., Lakshmi, V., Chan, T. K., and Nghiem, S. V.: Soil moisture retrieval from AMSR-E, IEEE transactions on Geoscience and remote sensing, 41, 215–229, 2003.

Ouatiki, H., Boudhar, A., Tramblay, Y., Jarlan, L., Benabdelouhab, T., Hanich, L., El Meslouhi, M. R., and Chehbouni, A.: Evaluation of TRMM 3B42 V7 Rainfall Product over the Oum Er Rbia Watershed in Morocco, Climate, 5, 1, 2017.

Parajka, J., Naeimi, V., Blöschl, G., Wagner, W., Merz, R., and Scipal, K.: Assimilating scatterometer soil moisture data into conceptual hydrologic models at the regional scale, Hydrology and Earth System Sciences Discussions, 10, 353–368, 2006.

Pearson, K.: Mathematical Contributions to the Theory of Evolution.–On a Form of Spurious Correlation Which May Arise When Indices Are Used in the Measurement of Organs, Proceedings of the royal society of london, 60, 489–498, 1896.

Prinzio, M. D., Castellarin, A., and Toth, E.: Data-driven catchment classification: application to the pub problem, Hydrology and Earth System Sciences, 15, 1921–1935, 2011.

Reichle, R. H. and Koster, R. D.: Bias reduction in short records of satellite soil moisture, Geophysical Research Letters, 31, 2004.

Rientjes, T., Muthuwatta, L. P., Bos, M., Booij, M., and Bhatti, H.: Multi-variable calibration of a semi-distributed hydrological model using streamflow data and satellite-based evapotranspiration, Journal of Hydrology, 505, 276–290, 2013.

Roy, A., Royer, A., and Turcotte, R.: Improvement of springtime streamflow simulations in a boreal environment by incorporating snow-covered area derived from remote sensing data, Journal of hydrology, 390, 35–44, 2010.

Samaniego, L., Bárdossy, A., and Kumar, R.: Streamflow prediction in ungauged catchments using copula-based dissimilarity measures, Water Resources Research, 46, 2010a.

Samaniego, L., Kumar, R., and Attinger, S.: Multiscale parameter regionalization of a grid-based hydrologic model at the mesoscale, Water Resources Research, 46, 2010b.

Schellekens, J. and Weiland, F. S.: earth2observe/downscaling-tools: 2017.2. Pre-release., doi:doi:10.5281/zenodo..545779, 2017.

Seibert, J. and Beven, K. J.: Gauging the ungauged basin: how many discharge measurements are needed?, Hydrology and Earth System Sciences, 13, 883–892, 2009.

Seneviratne, S. I., Corti, T., Davin, E. L., Hirschi, M., Jaeger, E. B., Lehner, I., Orlowsky, B., and Teuling, A. J.: Investigating soil moisture–climate interactions in a changing climate: A review, Earth-Science Reviews, 99, 125–161, 2010.

Sivapalan, M., Takeuchi, K., Franks, S., Gupta, V., Karambiri, H., Lakshmi, V., Liang, X., McDonnell, J., Mendiondo, E., O'connell, P., et al.: IAHS Decade on Predictions in Ungauged Basins (PUB), 2003–2012: Shaping an exciting future for the hydrological sciences, Hydrological sciences journal, 48, 857–880, 2003.

Sutanudjaja, E., Van Beek, L., De Jong, S., Van Geer, F., and Bierkens, M.: Large-scale groundwater modeling using global datasets: a test case for the Rhine-Meuse basin, Hydrology and Earth System Sciences, 15, 2913–2935, 2011.

Sutanudjaja, E., Van Beek, L., De Jong, S., Van Geer, F., and Bierkens, M.: Calibrating a large-extent high-resolution coupled groundwater-land surface model using soil moisture and discharge data, Water Resources Research, 50, 687–705, 2014.

Sutanudjaja, E., van Beek, R., Wada, Y., Bosmans, J., Drost, N., de Graaf, I., de Jong, K., Lopez Lopez, P., Pessenteiner, S., Oliver, S., Straatsma, M., Wanders, N., Wisser, D., and Bierkens, M.: PCR-BLOBWB_model, Zenodo, doi:http://doi.org/10.5281/zenodo.60764, 2016.

Tapley, B. D., Bettadpur, S., Watkins, M., and Reigber, C.: The gravity recovery and climate experiment: Mission overview and early results, Geophysical Research Letters, 31, 2004.

Thirel, G., Salamon, P., Burek, P., and Kalas, M.: Assimilation of MODIS snow cover area data in a distributed hydrological model using the particle filter, Remote Sensing, 5, 5825–5850, 2013.

Tramblay, Y., Bouaicha, R., Brocca, L., Dorigo, W., Bouvier, C., Camici, S., and Servat, E.: Estimation of antecedent wetness conditions for flood modelling in northern Morocco, Hydrology and Earth System Sciences, 16, 4375, 2012.

Tramblay, Y., Thiemig, V., Dezetter, A., and Hanich, L.: Evaluation of satellite-based rainfall products for hydrological modelling in Morocco, Hydrological Sciences Journal, 61, 2509–2519, 2016.

Van Beek, L., Wada, Y., and Bierkens, M. F.: Global monthly water stress: 1. Water balance and water availability, Water Resources Research, 47, 2011.

Vereecken, H., Huisman, J., Bogena, H., Vanderborght, J., Vrugt, J., and Hopmans, J.: On the value of soil moisture measurements in vadose zone hydrology: A review, Water resources research, 44, 2008.

Wanders, N., Bierkens, M. F., de Jong, S. M., de Roo, A., and Karssenberg, D.: The benefits of using remotely sensed soil moisture in parameter identification of large-scale hydrological models, Water resources research, 50, 6874–6891, 2014.

Weedon, G. P., Balsamo, G., Bellouin, N., Gomes, S., Best, M. J., and Viterbo, P.: The WFDEI meteorological forcing data set: WATCH Forcing Data methodology applied to ERA-Interim reanalysis data, Water Resources Research, 50, 7505–7514, 2014.

Weiland, F. S., Lopez, P., Van Dijk, A., and Schellekens, J.: Global high-resolution reference potential evaporation, in: MODSIM 2015, Conference Proceedings, Broadbeach, Queensland, Australia, 2015.

Winsemius, H., Schaefli, B., Montanari, A., and Savenije, H.: On the calibration of hydrological models in ungauged basins: A framework for integrating hard and soft hydrological information, Water Resources Research, 45, 2009.

Yaeger, M., Coopersmith, E., Ye, S., Cheng, L., Viglione, A., and Sivapalan, M.: Exploring the physical controls of regional patterns of flow duration curves–Part 4: A synthesis of empirical analysis, process modeling and catchment classification, Hydrology and Earth System Sciences, 16, 4483–4498, 2012.

Table 1. Hydrological and geographical information of the analysed catchments at the Oum Er Rbia basin.

Station name	River	Upstream basin area (km^2)	Oulet location		Elevation (m AOD)
			Longitude	Latitude	
Ait Ouchene	El Abid	2350	-6.180	32.225	1070
Mechra Eddahk	Oum Er Rbia	6555	-6.52	32.435	406

Table 2. Calibration scenarios.

Scenario identifier	Description
S0	Reference scenario
S1	Calibration using in-situ observed discharge time series
S2	Calibration using GLEAM actual evapotranspiration times series
S3	Calibration using ESA CCI surface soil moisture time series
S4	Step-wise calibration: using GLEAM actual evapotranspiration and ESA CCI surface soil moisture time series

Table 3. Parameter values used in the calibration processes.

Parameters ID	Description	Prefactors	Parameter values
W_{min}	Minimum soil water capacity	$f_w \in \{0.75, 1, 1.25\}$	$W_{min} = f_w * W_{max}$
K_{sat1}	Saturated hydraulic conductivity of 1^{st} soil layer	$f_k \in \{-0.25, 0, 0.25\}$	$log(K_{sat1}) = f_k + log(K_{sat1_{ref}})$
K_{sat2}	Saturated hydraulic conductivity of 2^{nd} soil layer	$f_k \in \{-0.25, 0, 0.25\}$	$log(K_{sat2}) = f_k + log(K_{sat2_{ref}})$
K_{sat3}	Saturated hydraulic conductivity of 3^{rd} soil layer	$f_k \in \{-0.25, 0, 0.25\}$	$log(K_{sat3}) = f_k + log(K_{sat3_{ref}})$
J	Baseflow recession coefficient	$f_j \in \{-0.5, 0, 0.5\}$	$log(J) = f_j + log(J_{ref})$
$E_{p,0}$	Reference potential evapotranspiration	$f_e \in \{0.75, 1, 1.25\}$	$E_{p,0} = f_e * E_{p,0_{ref}}$

Table 4. Parameter identifiabilities and optimal values for each calibration scenario.

Calibration scenario	f_e	f_j	f_k	f_w	KGE (Ait Ouchene)	KGE (Mechra Eddahk)
S0	1	0	0	1	0.470 / -1.906 / -0.542**	0.607 / 0.325 / 0.561
S1	1.25	NI*	NI	1.25	0.510 / -0.494 / 0.520	0.688 / 0.439 / 0.703
S2	1.25	NI	NI	NI	0.508 / -0.580 / 0.342	0.602 / 0.423 / 0.693
S3	NI	NI	0.25	1.25	0.487 / -0.607 / 0.331	0.634 / 0.369 / 0.613
S4	1.25	NI	0.25	1.25	0.478 / -0.768 / 0.271	0.522 / 0.328 / 0.573

*NI indicates that the parameter was not identifiable

**KGE values are obtained from observed and simulated discharge when PCR-GLOBWB is forced with EI / WFDEI / MSWEP

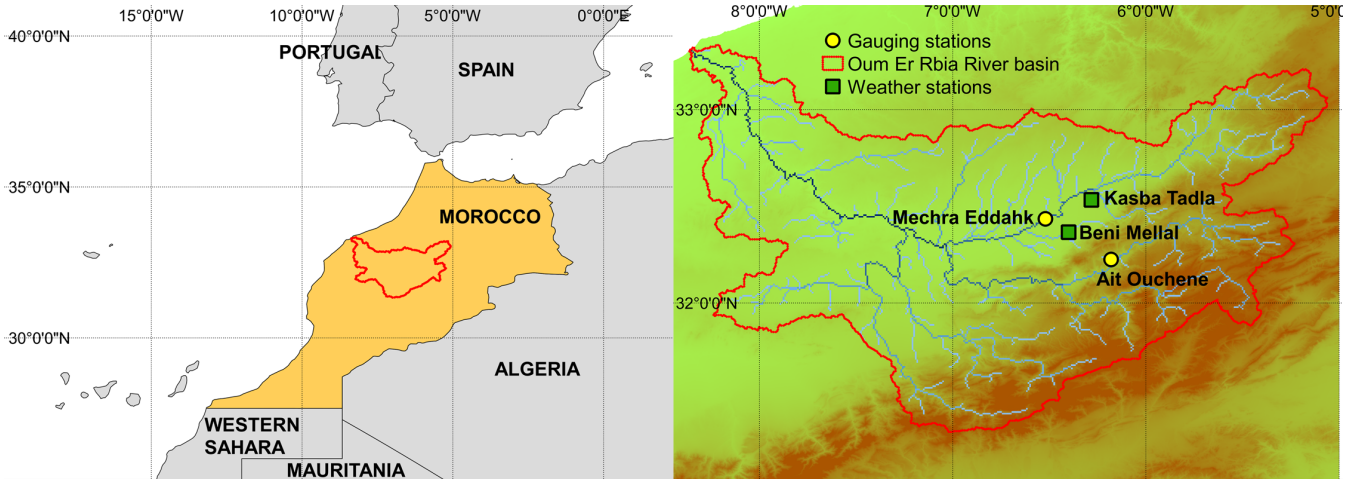

Figure 1. Oum Er Rbia River basin and its location in Morocco (The delineation of the catchment is physically based). Yellow points represent the gauging stations and green squares represent the weather stations.

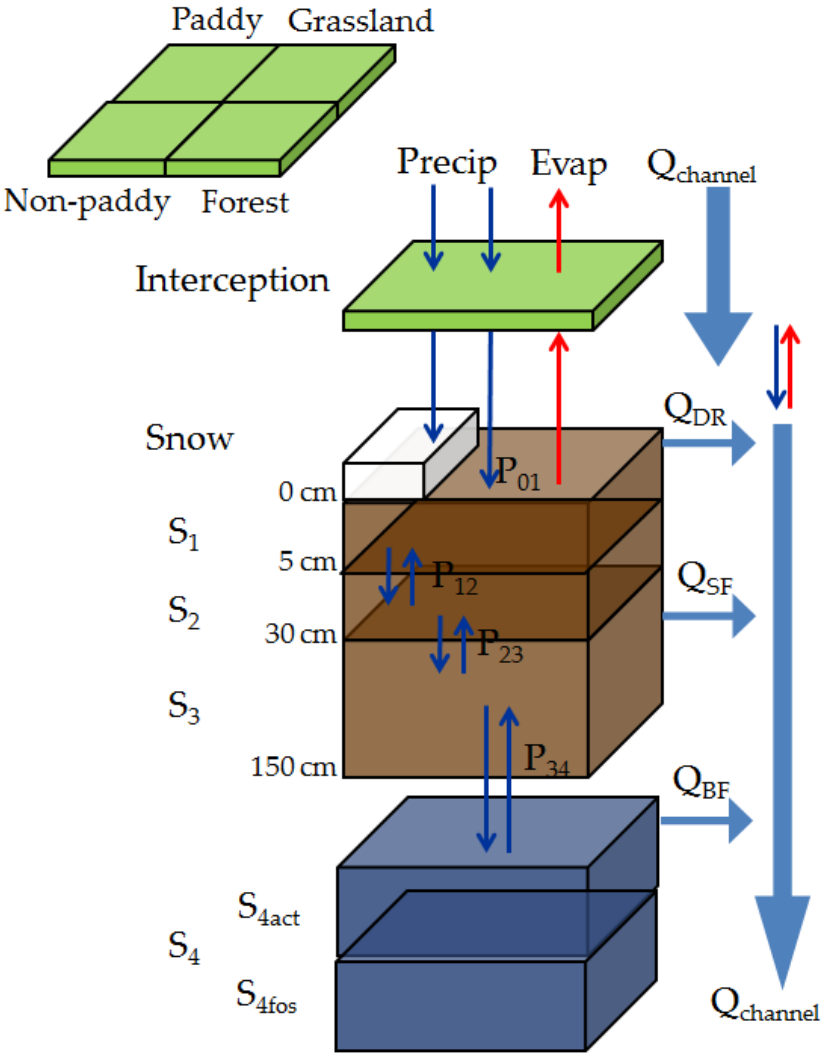

Figure 2. PCR-GLOBWB model structure, adapted from Van Beek et al. (2011).

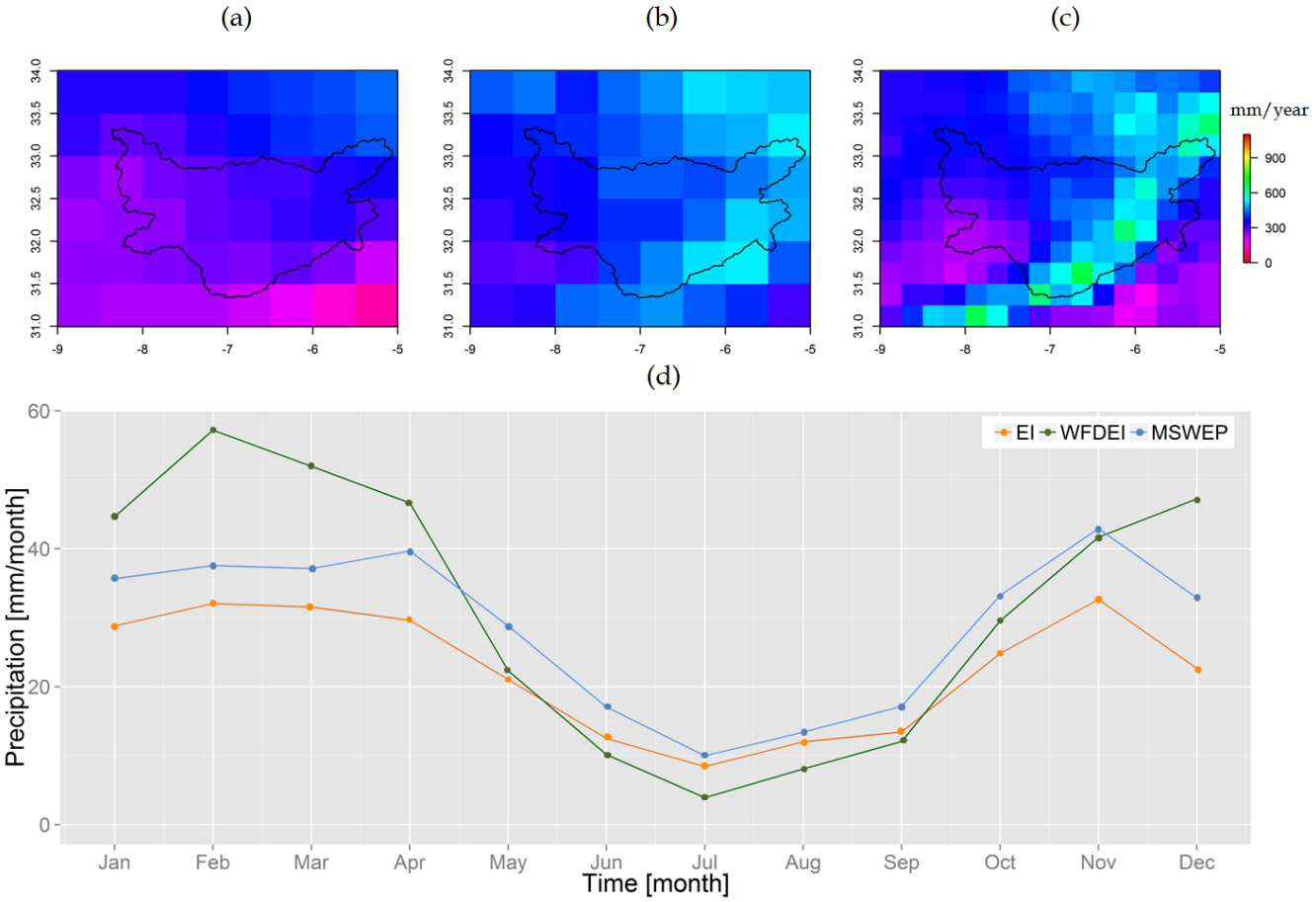

Figure 3. (a) EI annual mean precipitation, (b) WFDEI annual mean precipitation and (c) MSWEP annual mean precipitation for 1979-2010 time period and (d) climatology of EI, WFDEI and MSWEP precipitation products.

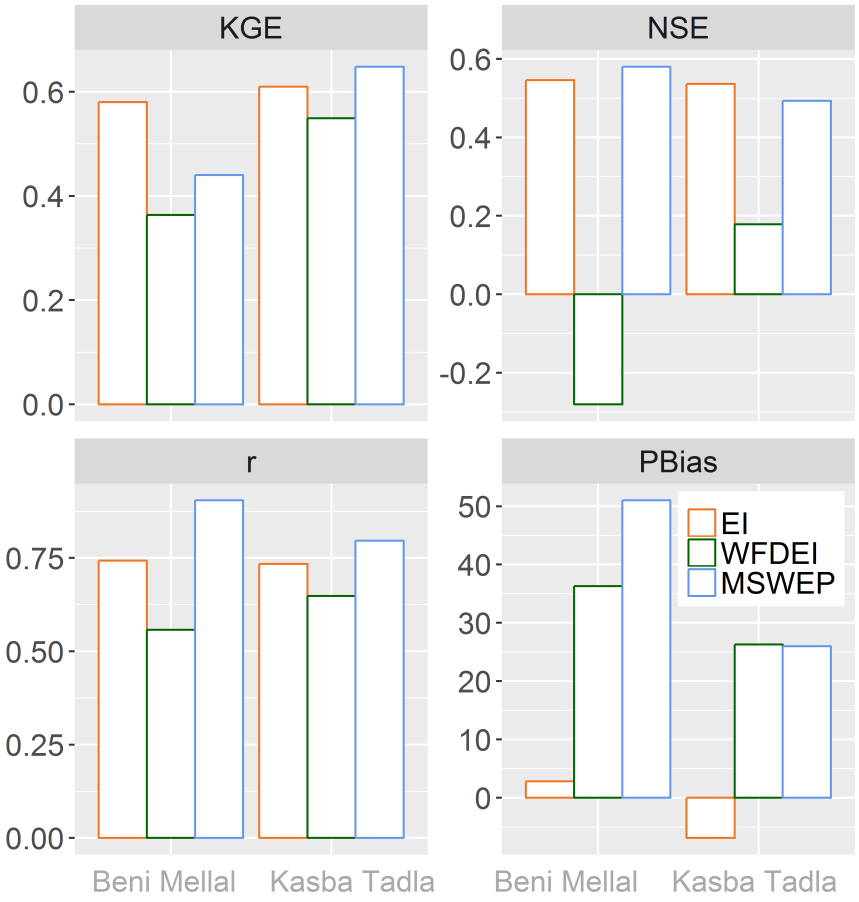

Figure 4. Performance metrics of daily EI, WFDEI and MSWEP precipitation products at Beni Mellal and Kasba Tadla weather stations, including Kling-Gupta efficiency (KGE), Nash-Sutcliffe efficiency (NSE), Pearson's correlation coefficient (r) and Percent Bias ($PBias$).

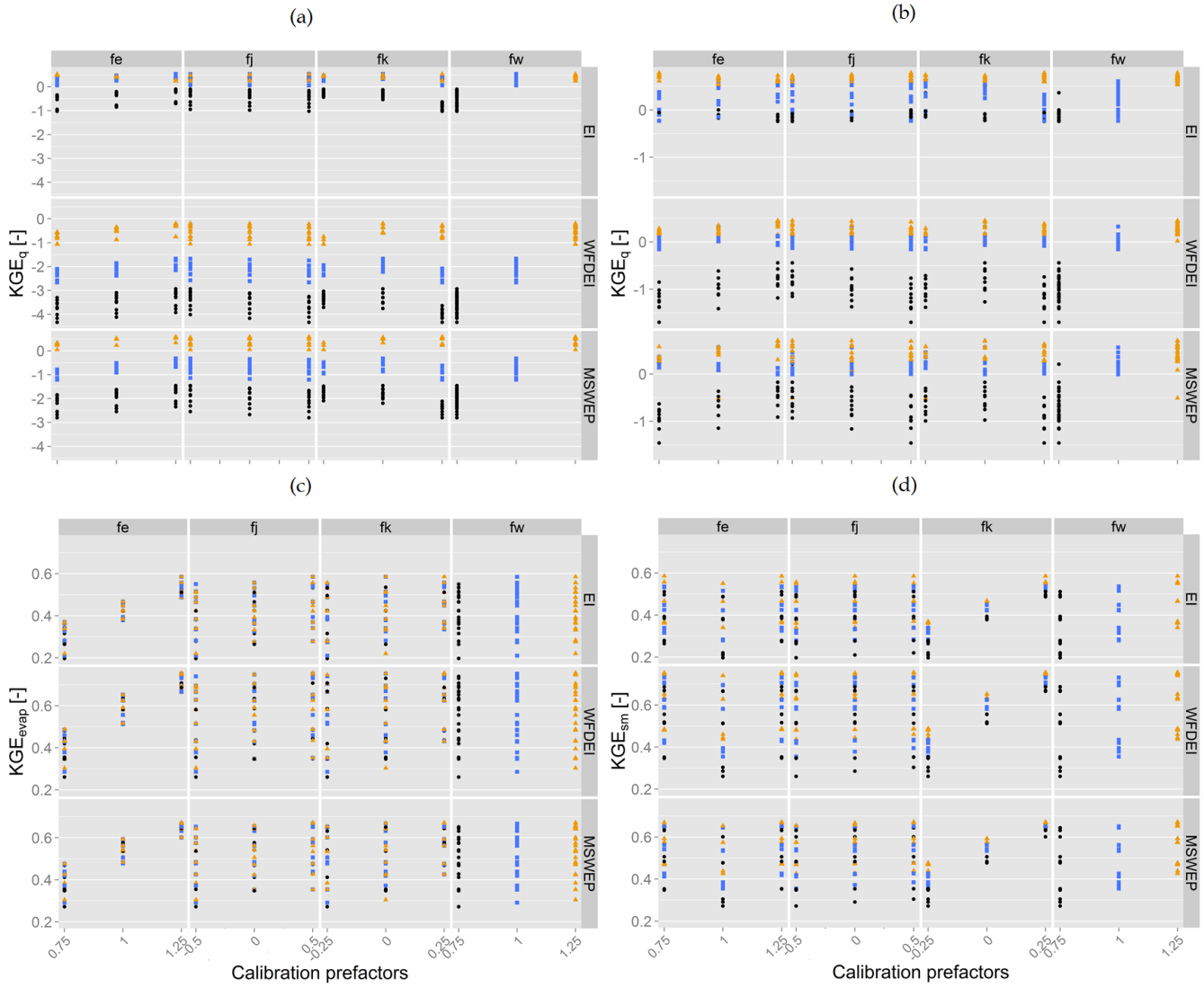

Figure 5. Scatterplots of discharge performance indicator KGE based on the monthly observations versus prefactors f_e, f_j, f_k and f_w for the calibration scenarios S1 ((a) Ait Ouchene (b) Mechra Eddahk), S2 (c) and S3 (d). In each sub-figure, columns indicate the different calibrated prefactors and rows indicate the three global precipitation products used as model forcing. Different colors and dot shapes indicate different f_w values.

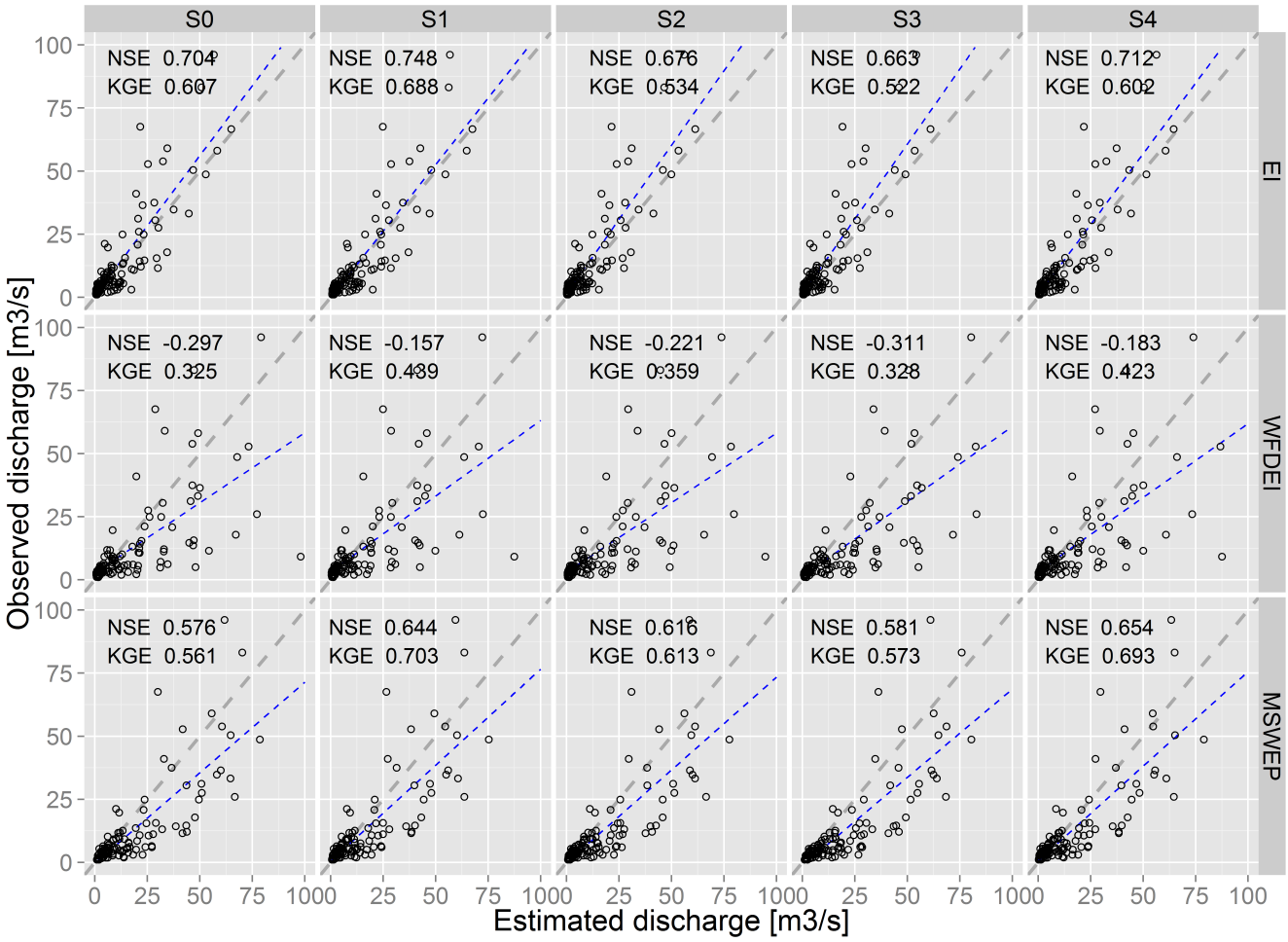

Figure 6. Scatterplots of monthly estimated discharge (x-axis) and observed discharge (y-axis) at Mechra Eddahk. Rows indicate the three global precipitation products and columns indicate the five calibration scenarios.

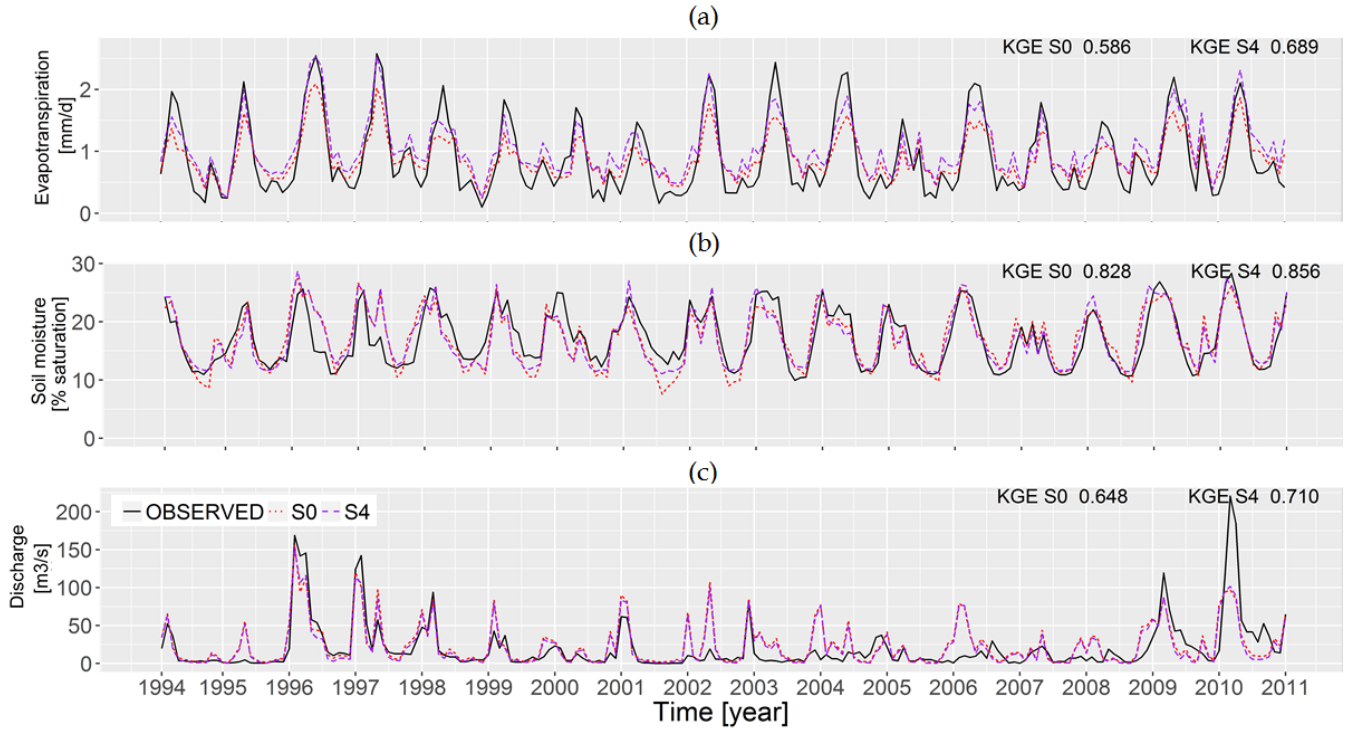

Figure 7. (a) Monthly GLEAM actual evapotranspiration (black) and estimated actual evapotranspiration (red and purple) time series over the entire Oum Er Rbia basin. (b) Monthly ESA CCI soil moisture (black) and estimated soil moisture (red and purple) time series over the entire Oum Er Rbia basin. (c) Monthly observed discharge (black) and estimated discharge (red and purple) time series at Mechra Eddahk. The red dashed lines represent estimates from calibration scenario S0 (reference scenario). The purple dashed lines represent the calibrated time series from calibration scenario S4 which are taken from the runs that yield the best simulations. Estimated time series over the entire Oum Er Rbia basin for the validation time period obtained with MSWEP precipitation are shown.

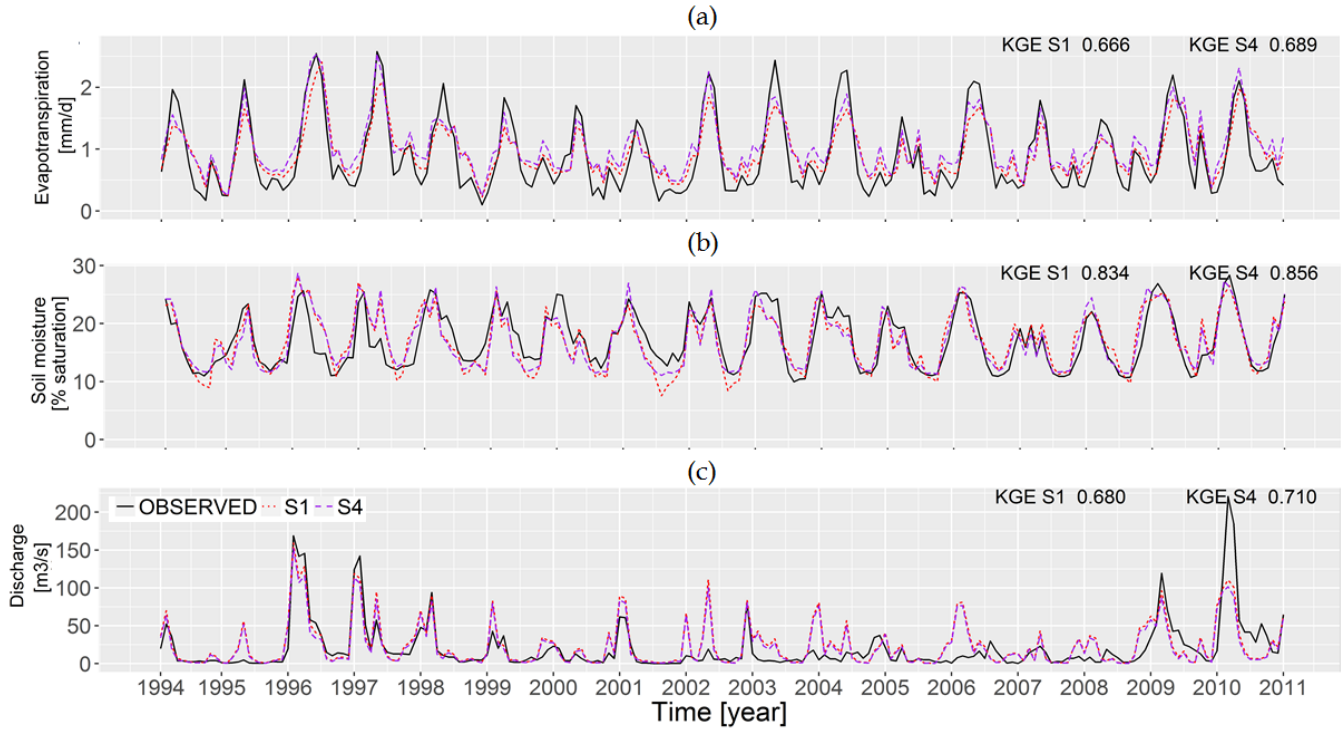

Figure 8. (a) Monthly GLEAM actual evapotranspiration (black) and estimated actual evapotranspiration (red and purple) time series over the entire Oum Er Rbia basin. (b) Monthly ESA CCI soil moisture (black) and estimated soil moisture (red and purple) time series over the entire Oum Er Rbia basin. (c) Monthly observed discharge (black) and estimated discharge (red and purple) time series at Mechra Eddahk. The red dashed lines represent estimates from calibration scenario S1. The purple dashed lines represent the calibrated time series from calibration scenario S4 which are taken from the runs that yield the best simulations. Estimated time series over the entire Oum Er Rbia basin for the validation time period obtained with MSWEP precipitation are shown.

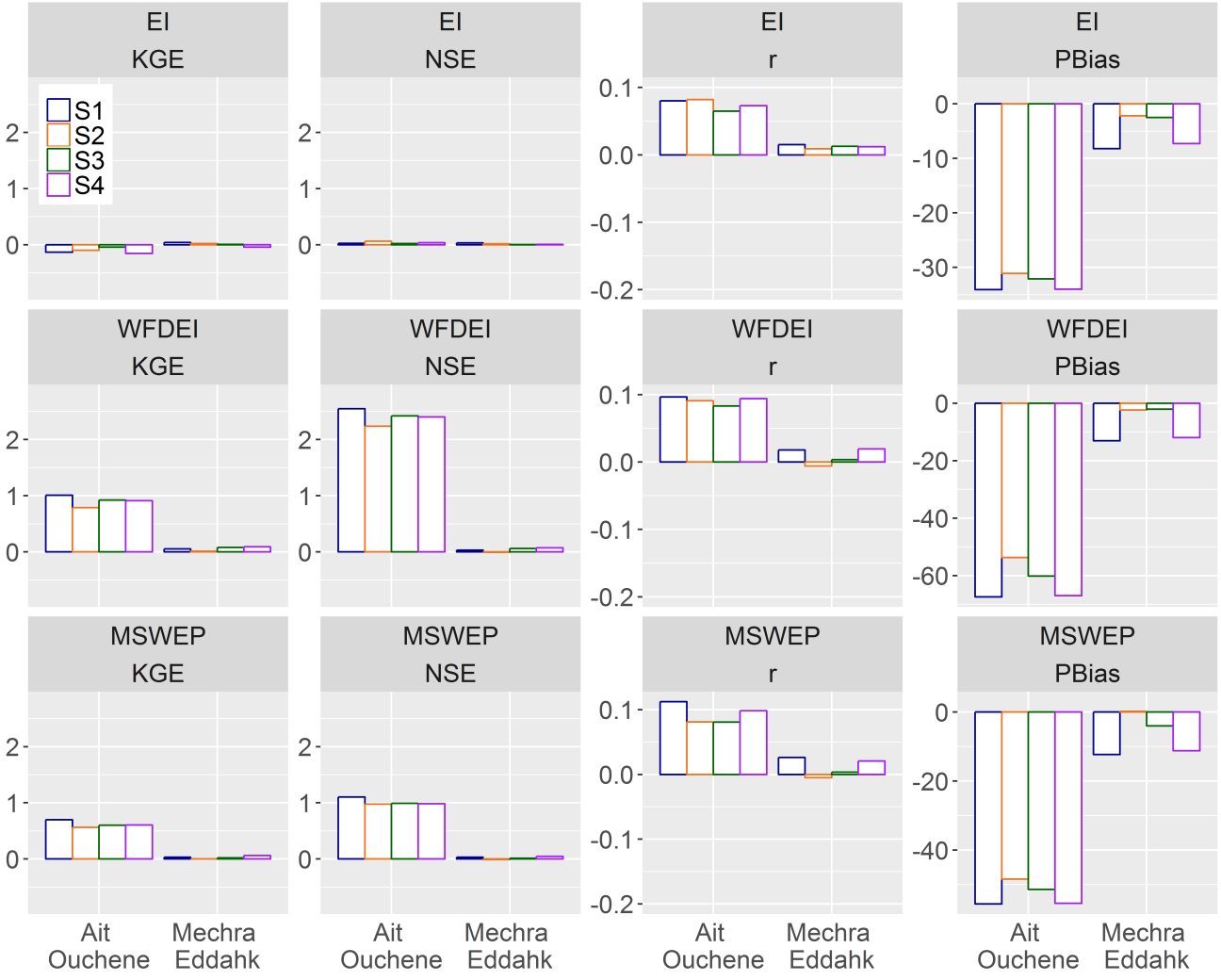

Figure 9. KGE, NSE, r and $PBias$ variations comparing monthly discharge estimates of calibration scenarios S1, S2, S3 and S4 with S0. Rows indicate the three global precipitation products and columns indicate the performance metrics.

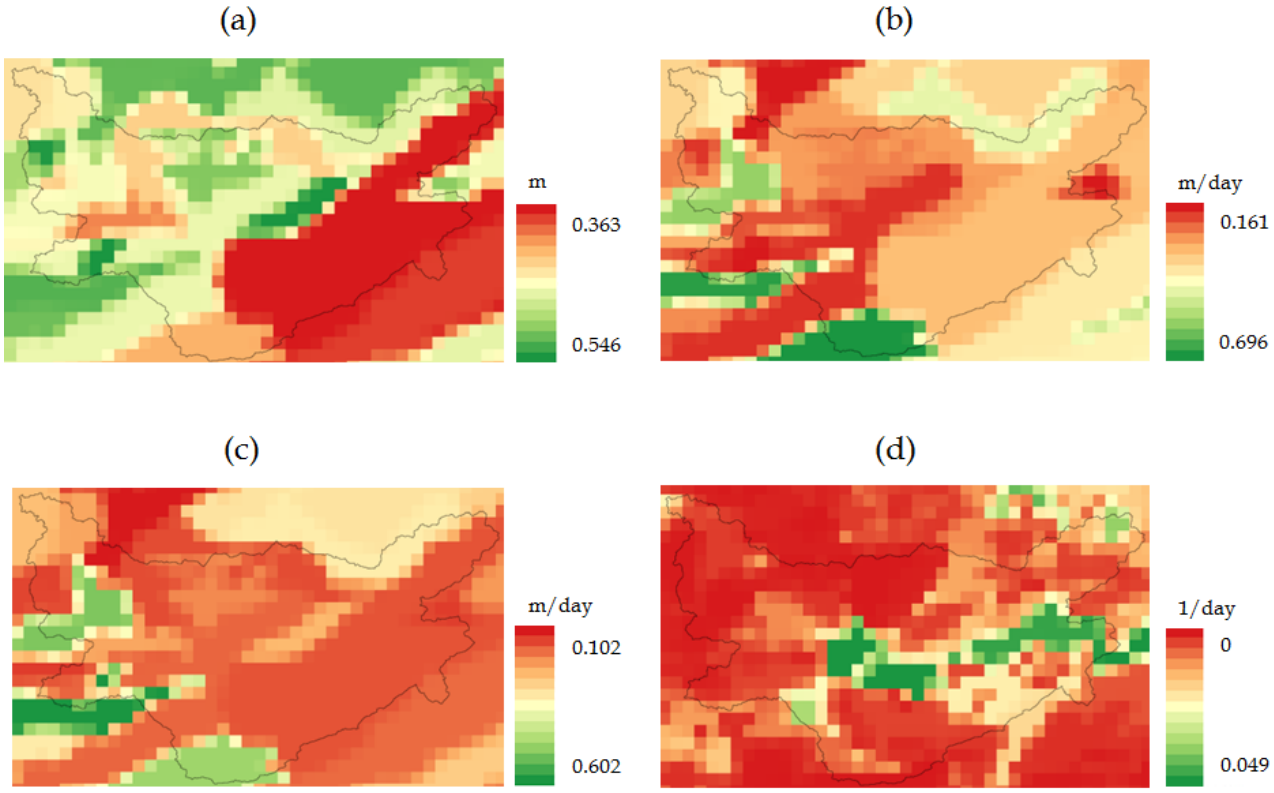

Figure A1. Initial model parameter values for the S0 calibration scenario (reference): (a) total soil water storage capacity ($W_{max} = SC_1 + SC_2 + SC_3$), (b) saturated hydraulic conductivity of the 1^{st} and 2^{nd} soil layers (K_{sat1} and K_{sat2}), (c) saturated hydraulic conductivity of 3^{rd} soil layer (K_{sat3}) and (d) baseflow recession coefficient (J).

Acknowledgements. This research received funding from the European Union Seventh Framework Programme (FP7/2007-2013) under grant agreement no. 603608, Global Earth Observation for integrated water resource assessment: eartH2Observe. We would like to thank ICARDA for their engagement and collaboration during this work. For the discharge data, we are very grateful to Yves Tramblay from the Institut de Recherche pour le Developpement (IRD) in France and El Mahdi El Khalki and Lahoucine Hanich from the Laboratoire de Géoressources, Département des Sciences de la Terre, Faculté des Sciences et Techniques, Université Cadi Ayyad in Marrakech in Morocco. For the GLEAM evapotranspiration data, we would like to thank VU Amsterdam in The Netherlands and Ghent University in Belgium. For the ESA CCI soil moisture, we are indebted to the Vienna University of Technology in Austria.